Dear Author,

Please, note that changes made to the HTML content will be added to the article before publication, but are not reflected in this PDF.

Note also that this file should not be used for submitting corrections.

AUTHOR QUERY FORM

ELSEVIER	**Journal: BRES** **Article Number: 44243**	**Please e-mail your responses and any corrections to:** **E-mail: corrections.esch@elsevier.macipd.com**

Dear Author,

Please check your proof carefully and mark all corrections at the appropriate place in the proof (e.g., by using on-screen annotation in the PDF file) or compile them in a separate list. Note: if you opt to annotate the file with software other than Adobe Reader then please also highlight the appropriate place in the PDF file. To ensure fast publication of your paper please return your corrections within 48 hours.

For correction or revision of any artwork, please consult http://www.elsevier.com/artworkinstructions.

Any queries or remarks that have arisen during the processing of your manuscript are listed below and highlighted by flags in the proof. Click on the Q link to go to the location in the proof.

Your article is registered as a regular item and is being processed for inclusion in a regular issue of the journal. If this is NOT correct and your article belongs to a Special Issue/Collection please contact p.baskaran@elsevier.com immediately prior to returning your corrections.

| Location in article	Query / Remark: click on the Q link to go Please insert your reply or correction at the corresponding line in the proof
Q1	Please confirm that given names and surnames have been identified correctly and are presented in the desired order.
Q2	Please complete and update the reference given here (preferably with a DOI if the publication data are not known): (Heng et al., in press). For references to articles that are to be included in the same (special) issue, please add the words 'this issue' wherever this occurs in the list and, if appropriate, in the text.
Q3	(Harris et al., 2015) has been changed to (Harris et al., 2014) in the text. Please check and correct if necessary.
Q4	Please validate/approve the sponsor name National Health and Medical Research Council, Australia; National Institute of Health, United States.
Q5	Figs. 6, 11, 12-14 have been submitted as color images; however, the captions have been reworded to ensure that they are meaningful when your article is reproduced both in color and in black and white. Please confirm if the changes made are ok.

Thank you for your assistance.

> Please check this box or indicate your approval
> if you have no corrections to make to the PDF file
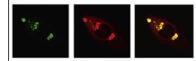
Highlights

Expansion of the lateral ventricles and ependymal deficits underlie the hydrocephalus evident in mice lacking the transcription factor NFIX

Brain Research ▮ (▮▮▮▮) ▮▮▮–▮▮▮

Diana Vidovic[a], Lachlan Harris[a], Tracey Harvey[a], Yee Hsieh Evelyn Heng[a], Aaron Smith[a], Jason Osinski[d], James Hughes[e], Paul Thomas[e], Richard M. Gronostajski[d], Timothy L. Bailey[c], Michael Piper[a,b]

[a] The School of Biomedical Sciences, The University of Queensland, Brisbane, Queensland 4072, Australia
[b] Queensland Brain Institute, The University of Queensland, Brisbane, Queensland 4072, Australia
[c] Institute for Molecular Bioscience, The University of Queensland, Brisbane, Queensland 4072, Australia
[d] Department of Biochemistry, Programs in Neuroscience and Genetics, Genomics & Bioinformatics, Developmental Genomics Group, New York State Center of Excellence in Bioinformatics and Life Sciences, State University of New York at Buffalo, New York 14203, USA
[e] School of Molecular and Biomedical Science, The University of Adelaide, Adelaide, South Australia 5005, Australia

- $Nfix^{-/-}$ mice develop hydrocephalus in the early postnatal period.
- NFIX can repress $Sox3$-promoter driven transcriptional activity.
- $Nfix^{-/-}$ mice exhibit normal development and function of the subcommissural organ.
- The ependymal layer of the lateral ventricles is abnormal in $Nfix^{-/-}$ mice.
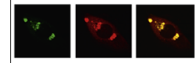
Research Report

Expansion of the lateral ventricles and ependymal deficits underlie the hydrocephalus evident in mice lacking the transcription factor NFIX

Diana Vidovic[a], Lachlan Harris[a], Tracey Harvey[a], Yee Hsieh Evelyn Heng[a], Aaron Smith[a], Jason Osinski[d], James Hughes[e], Paul Thomas[e], Richard M. Gronostajski[d], Timothy L. Bailey[c], Michael Piper[a,b,*]

[a]The School of Biomedical Sciences, The University of Queensland, Brisbane, Queensland 4072, Australia
[b]Queensland Brain Institute, The University of Queensland, Brisbane, Queensland 4072, Australia
[c]Institute for Molecular Bioscience, The University of Queensland, Brisbane, Queensland 4072, Australia
[d]Department of Biochemistry, Programs in Neuroscience and Genetics, Genomics & Bioinformatics, Developmental Genomics Group, New York State Center of Excellence in Bioinformatics and Life Sciences, State University of New York at Buffalo, New York 14203, USA
[e]School of Molecular and Biomedical Science, The University of Adelaide, Adelaide, South Australia 5005, Australia

ARTICLE INFO

ABSTRACT

Nuclear factor one X (NFIX) has been shown to play a pivotal role during the development of many regions of the brain, including the neocortex, the hippocampus and the cerebellum. Mechanistically, NFIX has been shown to promote neural stem cell differentiation through the activation of astrocyte-specific genes and via the repression of genes central to progenitor cell self-renewal. Interestingly, mice lacking Nfix also exhibit other phenotypes with respect to development of the central nervous system, and whose underlying causes have yet to be determined. Here we examine one of the phenotypes displayed by $Nfix^{-/-}$ mice, namely hydrocephalus. Through the examination of embryonic and postnatal $Nfix^{-/-}$ mice we reveal that hydrocephalus is first seen at around postnatal day (P) 10 in mice lacking Nfix, and is fully penetrant by P20. Furthermore, we examined the subcommissural organ (SCO), the Sylvian aqueduct and the ependymal layer of the lateral ventricles, regions that when malformed and functionally perturbed have previously been implicated in the development of hydrocephalus. SOX3 is a factor known to regulate SCO development. Although we revealed that NFIX could repress Sox3-promoter-driven transcriptional activity in vitro, SOX3 expression within the SCO was normal within $Nfix^{-/-}$ mice, and Nfix mutant mice showed no abnormalities in the structure or function of the SCO. Moreover, these mutant mice exhibited no overt blockage of the Sylvian aqueduct. However, the

*Corresponding author at: The School of Biomedical Sciences and the Queensland Brain Institute, The University of Queensland, Brisbane 4072, Australia. Fax: +61 7 3365 1766.
E-mail address: m.piper@uq.edu.au (M. Piper).

ependymal layer of the lateral ventricles was frequently absent in $Nfix^{-/-}$ mice, suggesting that this phenotype may underlie the development of hydrocephalus within these knockout mice.

1. Introduction

Hydrocephalus is a common neurological disorder with an estimated incidence of 1–3 cases per 1000 live births (Del Bigio, 2010). Hydrocephalus arises when cerebrospinal fluid (CSF) accumulates abnormally within the ventricular system, usually due to either an over production of CSF by the choroid plexus, or to a failure of CSF to drain from the subarachnoid spaces due to impaired function of the ependymal cilia (both known as communicating hydrocephalus) or, more commonly, due to a blockage occurring within the ventricular system (known as non-communicating hydrocephalus) (Perez-Figares et al., 2001).

At a cellular and molecular level, the precise causes underlying these different forms of hydrocephalus remain largely unknown. However, a common observation in many mouse models with non-communicating hydrocephalus is that they exhibit stenosis and occlusion of the Sylvian aqueduct (Perez-Figares et al., 2001). The Sylvian aqueduct joins the third and fourth ventricles, and, perhaps due to its narrowness, it is particularly prone to blockage. Indeed, stenosis of the Sylvian aqueduct is the most common site of intraventricular blockage within patients with hydrocephalus (Cinalli et al., 2011). The Sylvian aqueduct is kept open, or patent, in part via the production of a long, high molecular weight glycoprotein known as Reissner's fibre (Rodriguez et al., 1998). This fibre, composed primarily of highly glycosylated spondin, is produced by a specialised ependymal structure situated at the roof of the Sylvian aqueduct below the post-optic commissure known as the subcommissural organ (SCO) (Creveaux et al., 1998; Vio et al., 2008). Reissner's fibre extends from the SCO through the fourth ventricle to the end of the spinal cord central canal, maintaining the patency of the Sylvian aqueduct and so allowing CSF to flow through this bottleneck and into the fourth ventricle (Perez-Figares et al., 2001). Importantly, there are many examples of mice in which gene loss (Blackshear et al., 2003; Dietrich et al., 2009), or the over expression of transgenes (Lee et al., 2012; Louvi and Wassef, 2000), is accompanied by deficient SCO formation or Reissner's fibre production and hydrocephalus, implying that abnormal development of this structure plays a central role in aqueductal stenosis.

Many genes have been identified that play important roles during normal development of the nervous system, and that, when mutated or abnormally expressed, result in the development of hydrocephalus (Cinalli et al., 2011). $Nfix$ provides a salient example of this (Driller et al., 2007). $Nfix$ belongs to a group of genes known as the Nuclear factor one family, of which there are four isoforms within the vertebrate lineage, $Nfia$, $Nfib$, $Nfic$ and $Nfix$ (Heng et al., 2012; Mason et al., 2009). These genes encode site-specific
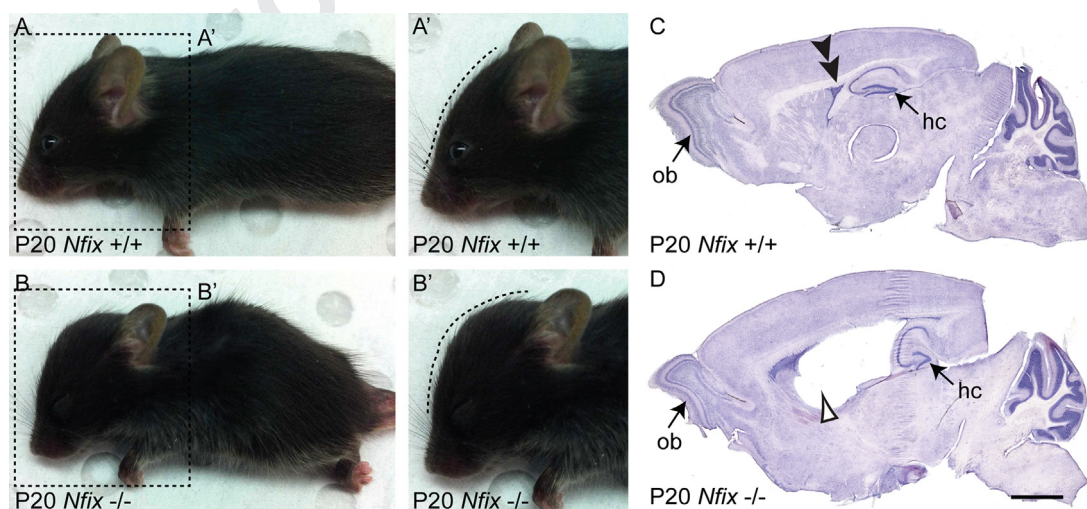
Fig. 1 – $Nfix^{-/-}$ mice exhibit hydrocephalus at weaning. At P20, wild-type mice (A) are markedly larger than $Nfix^{-/-}$ (B) littermate controls. Another phenotype evident in mice lacking $Nfix$ is the presence of a dome-shaped skull at this age (compare dotted lines in A' and B'). Hematoxylin stained sagittal sections of wild-type (C) and knockout (D) mice revealed a smaller olfactory bulb (ob) and a dysmorphic hippocampus (hc) within mutant mice. The lateral ventricle in wild-type mice at this sagittal plane was very small (double arrowhead in C), whereas there was massive expansion of the lateral ventricle within mutant mice (open arrowhead in D). Scale bar (in D): (A and B) 5 mm; (A' and B') 2.5 mm; (C and D) 1 mm.
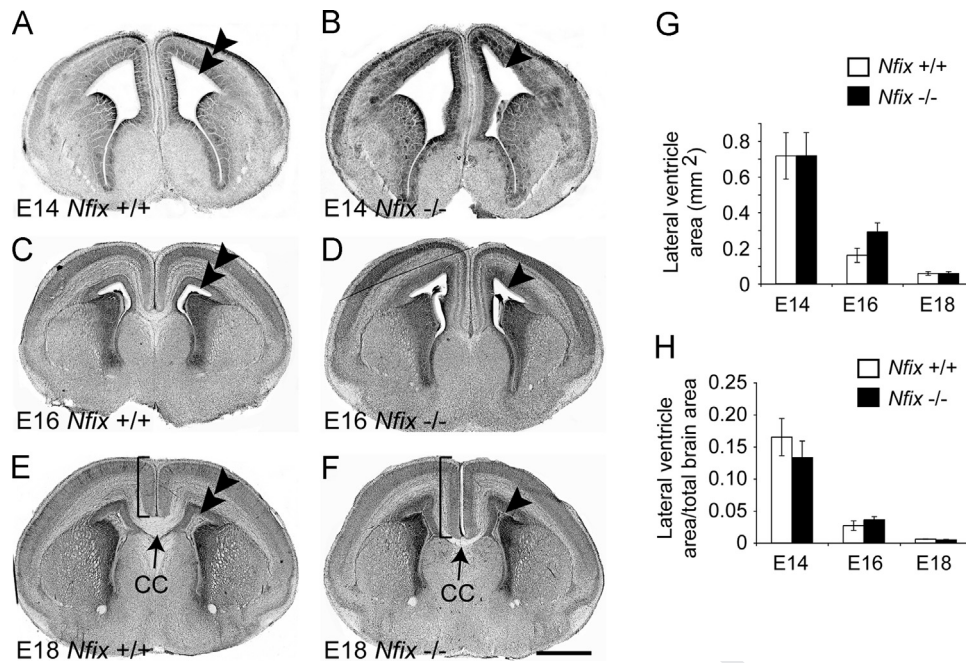
Fig. 2 – Nfix$^{-/-}$ mice do not exhibit ventricular enlargement during embryogenesis. Hematoxylin-stained coronal sections of E14, E16 and E18 wild-type (A, C and E) and Nfix$^{-/-}$ mice (B, D and F) at the level of the developing corpus callosum (CC). Although the corpus callosum was reduced in Nfix$^{-/-}$ mice, and the cingulate cortex was expanded (compare brackets in E and F), there was not any appreciable difference in the size of the lateral ventricles in comparison to controls (compare double arrowheads in A, C, E to arrowheads in B, D, and F). In support of this, quantification of total lateral ventricle area (G) and lateral ventricle area as a proportion of total brain area (H) did not reveal any difference between sample groups ($p > 0.05$, t-test). Scale bar (in F): (A and B) 300 μm; (C and D) 350 μm; (E and F) 500 μm.

transcription factors that have been implicated in regulating key aspects of nervous system development (Harris et al., 2014). For instance, NFIX has been shown to mediate normal development of the neocortex (Campbell et al., 2008), hippocampus (Heng et al., 2014a) and cerebellum (Piper et al., 2011), in part through promoting neural progenitor cell differentiation via the transcriptional repression of genes involved in progenitor cell self-renewal, such as Sox9 (Heng et al., 2014a). Interestingly, mice lacking Nfix survive until weaning, and have been reported to exhibit hydrocephalus (Campbell et al., 2008; Driller et al., 2007). However, the factors contributing to this phenotype in Nfix knockout mice remain undefined. Here we analysed the development of hydrocephalus in Nfix$^{-/-}$ mice, revealing that this phenotype becomes evident within the early postnatal period. Moreover, we reveal that the SCO appears to develop normally in the absence of Nfix, that Reissner's fibre is produced by the ependymal cells of the SCO in mutant mice, and that stenosis of the third ventricle is not evident within Nfix$^{-/-}$ mice. Finally, we reveal that the walls of the lateral ventricles are frequently denuded of their ependymal cell layer in Nfix mutant mice. Collectively, these data suggest that Nfix$^{-/-}$ mice exhibit communicating hydrocephalus, and that the hydrocephalic phenotype displayed by this strain of mice, rather than resulting from intraventricular blockage of the Sylvian aqueduct, more likely arises from aberrant loss of the ependymal cells that line the lateral ventricles.

2. Results

2.1. Nfix$^{-/-}$ mice exhibit hydrocephalus at weaning

Previous studies have shown that mice lacking Nfix exhibit hydrocephalus at P23 (Driller et al., 2007). We confirmed these findings through the analysis of Nfix$^{-/-}$ mice at P20. Comparison of the heads of wild-type and mutant mice at this age revealed marked differences, with Nfix$^{-/-}$ mice exhibiting a more dome-shaped skull when compared to littermate controls (compare the dotted lines in Fig. 1A' and B'). This was likely due to hydrocephalus, as the analysis of sagittal sections of these brains revealed greatly enlarged lateral ventricles in mice lacking Nfix (Fig. 1C and D). These data confirm the presence of postnatal hydrocephalus in this line of knockout mice, leading us to investigate the causes underlying the development of this phenotype in more detail.

2.2. Hydrocephalus develops postnatally in mice lacking Nfix

To determine when hydrocephalus first became evident within Nfix$^{-/-}$ mice we performed hematoxylin staining on coronal sections of littermate wild-type and mutant brains at ages ranging between E14 and P20. We focussed our analysis at the level of the developing corpus callosum, as the lateral ventricles are easily observed at this position along the
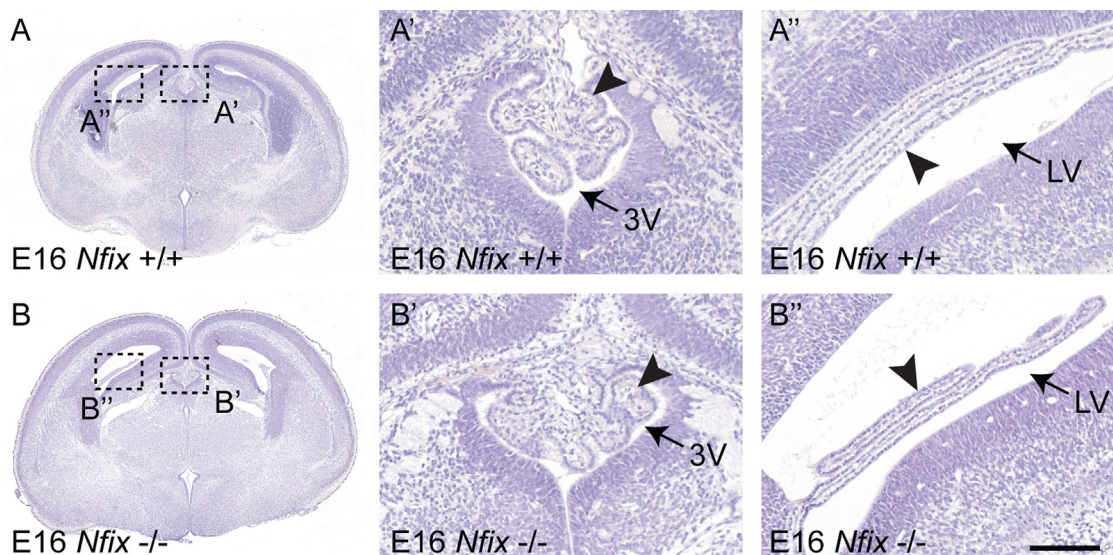
Fig. 3 – Normal appearance of the choroid plexus in embryonic $Nfix^{-/-}$ mice. Coronal paraffin sections (6 μm) of E16 wild-type (A) and $Nfix^{-/-}$ (B) mice stained with hematoxylin. Within both the third ventricle (3 V; A' and B') and the lateral ventricle (LV; A" and B"), the choroid plexus can be observed (arrowheads). We observed no morphological abnormalities within the choroid plexus of mice lacking $Nfix$. Scale bar (in B"): (A and B) 350 μm; (A', B', A", and B") 50 μm.

rostro-caudal axis of the telencephalon. Between the ages of E14 and E18, we did not observe any appreciable differences in the size of the lateral ventricles between wild-type and mutant brains (Fig. 2A–F), nor did we observe any instances of denudation of the neuroepithelial ventricular zone within the lateral ventricles at these ages. Moreover, quantification of the total ventricular area, as well as ventricular area as a proportion of total brain area, did not reveal any significant differences in the size of the lateral ventricles between sample groups (Fig. 2G and H). The choroid plexus of the lateral ventricles and the third ventricle also appeared morphologically normal in $Nfix^{-/-}$ mice during embryonic stages (Fig. 3). Similarly, at both P2 and P5, we did not observe any evidence of lateral ventricular dilation within $Nfix^{-/-}$ mice (data not shown). However, at P10, we observed that 4 out of 8 mice lacking $Nfix$ exhibited expansion of the lateral ventricles (Fig. 4A and B). This phenotype became more pronounced between P15 and P20, with all $Nfix^{-/-}$ mice examined exhibiting significantly larger lateral ventricles in comparison to controls (Fig. 4C–H). $Nfix^{\pm}$ mice did not exhibit evidence of hydrocephalus at any of these ages (data not shown). Collectively, these data suggest that hydrocephalus develops postnatally within $Nfix^{-/-}$ mice.

2.3. Double heterozygous NFI mice exhibit progressively worsening hydrocephalus

$Nfix^{-/-}$ mice die soon after weaning, from as yet unknown causes, precluding the ongoing trajectory of hydrocephalic development to be tracked with these mice (Heng et al., 2014a). However, mice heterozygous for both $Nfib$ and $Nfix$ also exhibit hydrocephalus and survive beyond this age, enabling us to ask how hydrocephalus develops over time in mice heterozygous for two Nfi genes. As with homozygous $Nfix$ mutants (Fig. 4D), hydrocephalus was evident within $Nfib^{\pm}$; $Nfix^{\pm}$ mice at P10, with these mice displaying enlarged

lateral ventricles at this age (Fig. 5A, B), a phenotype also seen at P20 (Fig. 5C and D). By P37, the hydrocephalic phenotype of the double heterozygotes had worsened. At the level of the corpus callosum, the lateral ventricles were very large and the corpus callosum was phenotypically absent (Fig. 5E and F). More caudally, at the level of the hippocampus, the ventricles were hugely dilated in the double heterozygote, and the hippocampus and thalamus were diminished in comparison to the controls (Fig. 5G and H). These data suggest that hydrocephalus continues to worsen in the postnatal period in mice heterozygous for two Nfi genes.
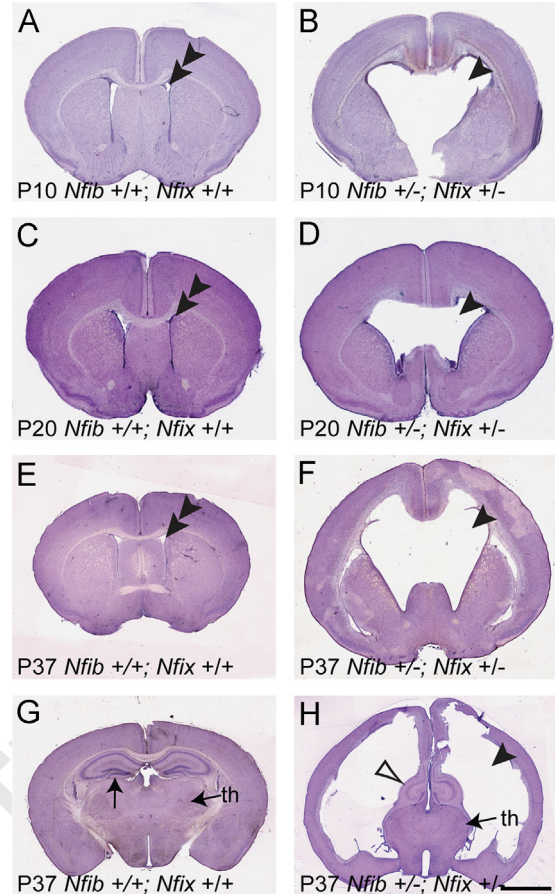
2.4. NFIX is expressed within the SCO

We next sought to determine the underlying cause of the postnatal hydrocephalus within $Nfix^{-/-}$ mice. There are multiple potential causes for hydrocephalus, however, stenosis of the Sylvian aqueduct is the most common site of intraventricular blockage leading to hydrocephalus (Cinalli et al., 2011). The aqueduct, which connects the third and fourth ventricles, is kept patent via the production of Reissner's fibre, a glycoprotein primarily comprised of spondin, that is secreted by a specialised gland at the roof of the diencephalon known as the SCO (Vio et al., 2008). Given a recent report demonstrating that ependymal cells within the developing telencephalon express NFIX (Campbell et al., 2008; Heng et al., in press), we first determined whether NFIX was expressed by ependymal cells within the SCO. Using an antibody specific for NFIX (Harris et al., 2013) on tissue from E14, E16 and E18 wild-type mice, we revealed that cells lining the walls of the third ventricle do indeed express NFIX (Fig. 6A, and C–F and data not shown). Importantly, at all of these ages, the SCO was strongly immunoreactive for NFIX (Fig. 6A), indicating that this transcription factor may regulate the development of this organ. The molecular determinants of SCO development are poorly understood, but recent
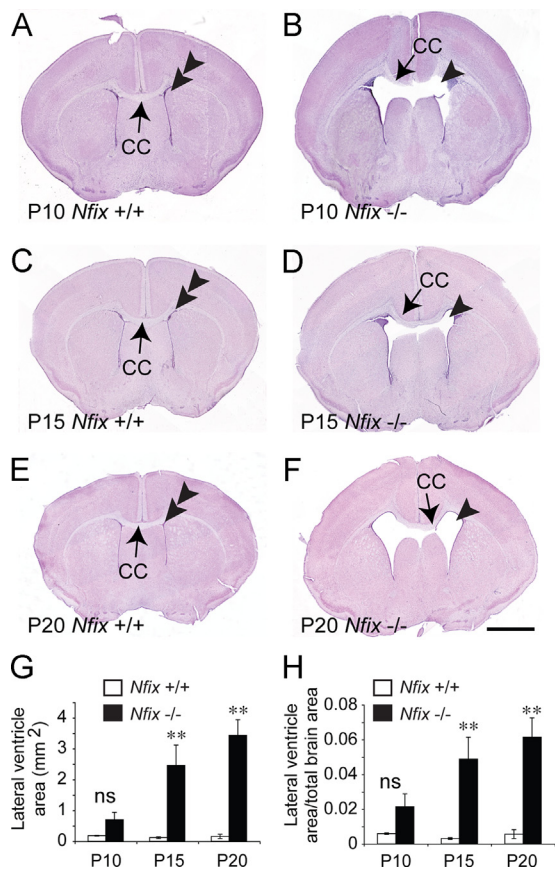
Fig. 4 – Hydrocephalus develops early in the postnatal period in $Nfix^{-/-}$ mice. Hematoxylin-stained coronal sections of P10, P15 and P20 wild-type (A, C and E) and $Nfix^{-/-}$ mice (B, D and F) at the level of the corpus callosum (CC). At P10, the lateral ventricles of $Nfix^{-/-}$ mice were frequently enlarged in comparison to controls (4 from 8 knockout mice), a phenotype recapitulated at P15 and P20 compare arrowheads in B, D and F with double arrowheads in A, C and E. Quantification of total lateral ventricle area (G) and lateral ventricle area as a proportion of total brain area (H) revealed that there was a significant increase in lateral ventricular size within $Nfix^{-/-}$ mice in comparison to controls at P15 and P20 ($^{**}p < 0.01$, t-test). ns = not significant. Scale bar (in F): (A and B) 500 μm; (C–F) 600 μm.

Fig. 5 – Continued progression of hydrocephalus in $Nfib^{\pm}$; $Nfix^{\pm}$ mice. Hematoxylin-stained coronal sections of P10, P20 and P37 wild-type (A, C, E and G) and $Nfib^{\pm}$; $Nfix^{\pm}$ (B, D, F and H) mice. Mice lacking two Nfi alleles exhibited marked expansion of the lateral ventricles at the level of the corpus callosum at all of these ages in comparison to controls (compare arrowheads in B, D and F with double arrowheads in A, C and E). More caudally, at the level of the hippocampus, the expansion of the lateral ventricles of $Nfib^{\pm}$; $Nfix^{\pm}$ mice was even more marked (arrowhead in H). Moreover, the hippocampus was dramatically reduced in the mutant (compare open arrowhead in H with the arrow in G), as was the thalamus (th). Scale bar (in H): (A and B) 500 μm; (C and D) 600 μm; (E–H) 750 μm.

findings have begun to elucidate the factors that mediate its formation. For example, the transcription factor $Sox3$ has been implicated in SCO development, with a transgenic line that expresses elevated levels of SOX3 exhibiting aberrant SCO development and hydrocephalus (Lee et al., 2012). We confirmed the expression of SOX3 by cells within the developing SCO at E18 (Fig. 6B), and, moreover, demonstrated that NFIX and SOX3 were co-expressed by cells within the nascent SCO using co-immunofluorescence labelling and confocal microscopy (Fig. 6C–F). Interestingly, we have previously revealed that other Sox family members, namely $Sox9$ and Bbx, are targets for transcriptional repression by NFIX during development of the dorsal telencephalon (Dixon et al., 2013; Heng et al., 2014a). Moreover, a microarray analysis performed in the latter study on hippocampi isolated from E16 wild-type and $Nfix^{-/-}$ mice revealed that $Sox3$ expression

within the hippocampus of $Nfix^{-/-}$ mice was significantly upregulated in comparison to controls (Heng et al., 2014a). Given these findings, and that NFIX and SOX3 are co-expressed within the SCO, we hypothesised that $Sox3$ could be a target for transcriptional repression by NFIX during SCO development, and that $Sox3$ upregulation in $Nfix^{-/-}$ mice may contribute to the postnatal hydrocephalus evident in these knockout mice.

To test this hypothesis we first validated our microarray findings. SOX3 is expressed by radial glial progenitor cells within the proliferative ventricular zone within the developing telencephalon (Rogers et al., 2013). Analysis of SOX3 expression within the neocortex and hippocampus of E16 wild-type and $Nfix^{-/-}$ mice revealed significantly more cells within the ventricular zone expressing SOX3 within $Nfix$ mutant mice (Supp. Fig. 1A–C),
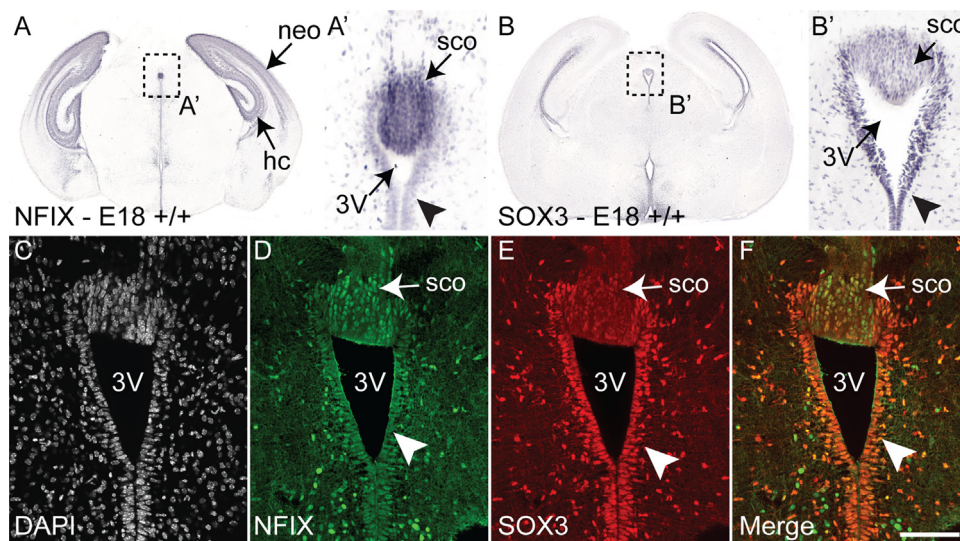
Fig. 6 – NFIX and SOX3 are co-expressed within the embryonic SCO. (A and B) Coronal sections of E18 wild-type mice revealing the expression of NFIX (A) and SOX3 (B). NFIX immunoreactivity was observed by cells within the neocortex (neo) and hippocampus (hc). Ependymal cells lining the walls of the third ventricle (3 V) were also immunopositive for both NFIX and SOX3 (arrowheads in A' and B'). Ependymal cells comprising the subcommissural organ (SCO), which is located at the roof of the third ventricle, were also expressed NFIX (A') and SOX3 (B'). (C–F) Co-immunofluorescence labelling and confocal microscopy (3.0 μm optical section) were used to demonstrate that NFIX (D; green) and SOX3 (E; red) were co-expressed by ependymal cells lining the walls of the third ventricle (arrowheads in D–F), as well as by cells of the SCO, at E18. Nuclei are labelled with DAPI (C; white). Scale bar (in F): (A and B) 500 μm; (A', B', and C–F) 50 μm. (For interpretation of the references to color in this figure legend, the reader is referred to the web version of this article.)

Table 1 – Putative NFI binding sites within the promoters of genes implicated in ependymal cell function. All potential NFI binding sites with p-values $\leq 10^{-4}$ were reported in the region of -3000 base pairs to $+200$ base pairs relative to the transcription start site (TSS) of the selected genes.

Gene	UCSC identifier	Position relative to TSS	Site p-value	Site sequence
Sox3	uc009vff.1	−27	1.9×10^{-5}	CGGGCAGGCTTCCCG
Sox3	uc009vff.1	−471	3.0×10^{-5}	CTGGAAAGCTCCCCG
Sox3	uc009vff.1	−745	8.7×10^{-5}	CTGGAAAGCTCCCCG
Sox3	uc009vff.1	−1237	9.2×10^{-5}	TGGGTTATCTGCCAA
Sox3	uc009vff.1	−2085	7.7×10^{-5}	GAGGGCAAGGGCCAG
Sox3	uc009vff.1	−2235	6.0×10^{-5}	TTGGAAAGAATCCTG
Celsr2	uc008qyx.1	194	2.1×10^{-5}	CTGGTGTAGAGCCAG
Celsr2	uc008qyz.1	−18	6.8×10^{-5}	GAGGGAAGAAGCCAA
Celsr2	uc008qyx.1	−140	1.8×10^{-5}	TGGGCCTGCACCCAG
Celsr2	uc008qyx.1	−430	7.3×10^{-5}	ATGGCCCTGCGCCAC
Celsr2	uc008qyz.1	−1503	1.7×10^{-5}	AGGGCAGGGTGCCAC
Celsr2	uc008qyz.1	−2135	7.7×10^{-5}	CGGGGGCCAGTGCCAC
Celsr2	uc008qyz.1	−2141	2.8×10^{-5}	GGGGGACGGGGCCAG
Celsr2	uc008qyz.1	−2261	3.8×10^{-5}	CTGGCCAGATCCCTG
Celsr3	uc009rrc.1	−37	2.4×10^{-5}	TAGGCCTGGAGCCTG
Celsr3	uc009rrb.1	−60	1.5×10^{-5}	CGGGCCTTGGGCCCG
Celsr3	uc009rrb.1	−194	1.4×10^{-5}	GGGGCCGGTATGCCAA
Celsr3	uc009rrb.1	−1420	2.1×10^{-5}	CTGGCCCGCCCCCAA
Celsr3	uc009rrc.1	−1578	1.1×10^{-7}	GTGGCCAGGTGCCAA
Cdh2	uc008edx.2	−2198	6.9×10^{-6}	CGGGCAAGAATCCAA
Dvl2	uc007jtl.1	−281	9.1×10^{-6}	GGGGCCGAGTCCCAG

corroborating our earlier microarray findings. Further evidence to support a direct role for NFIX in the transcriptional regulation of Sox3 came from a bioinformatic screen aimed at identifying NFI consensus binding motifs. This in silico screen identified six putative NFI binding sites within the region 3000 base pairs upstream of the Sox3 transcription start site (at −2235, −2085, −1237, −745, −471 and −27 relative to the transcription start site; Table 1). Next, we used a reporter gene assay to determine the ability of NFIX to regulate Sox3 promoter-driven transcriptional activity. A 1278 base pair fragment of the mouse Sox3 promoter containing the four putative NFI binding motifs most proximal to the transcription start site was able to induce
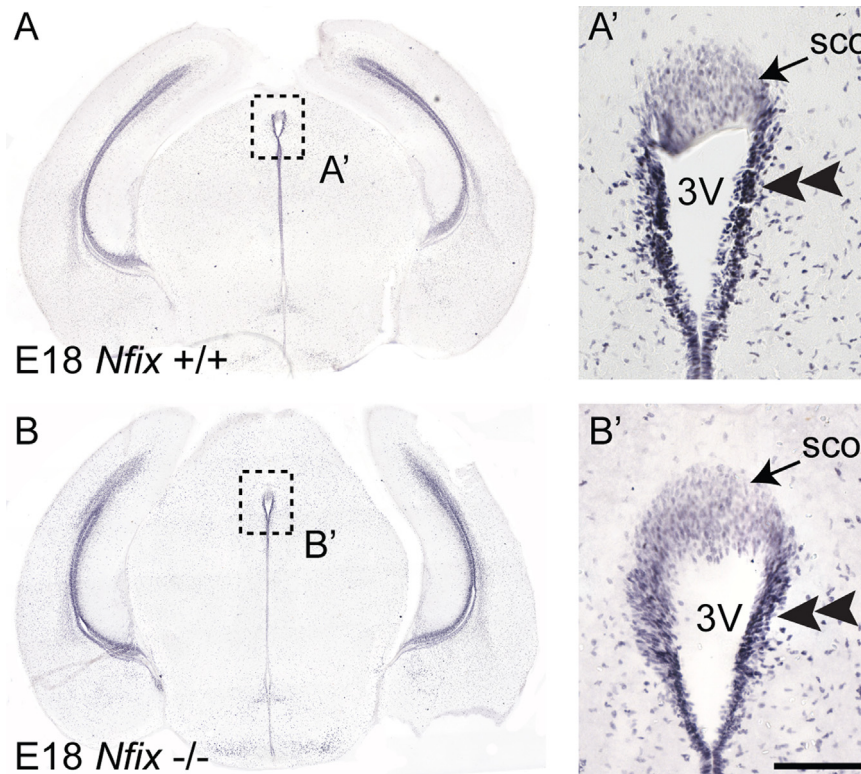
Fig. 7 – SOX3 expression is not altered within the SCO of $Nfix^{-/-}$ mice. Coronal sections of E18 wild-type (A) and $Nfix^{-/-}$ (B) mice revealing the expression of SOX3. Within the wild-type and the mutant, cells lining the walls of the third (3 V) ventricle expressed high levels of SOX3 (double arrowheads in A' and B'). Ependymal cells within the SCO expressed SOX3 at a lower level in the wild-type in comparison to cells lining the walls of the third ventricle (A'). Expression of SOX3 by cells within the SCO of $Nfix^{-/-}$ mice was comparable to the control (B'). Scale bar (in F): (A and B) 500 μm; (A', B', and C–F) 50 μm.

reporter gene (luciferase) activity in NeuroA cells (Suppl. Fig. 1D). Co-transfection of NFIX with the Sox3 promoter construct culminated in significantly reduced levels of luciferase expression, a finding replicated in a second neuronal cell line, NSC34 (Suppl. Fig. 1D). In total, these findings indicate that, at least within the dorsal telencephalon, Sox3 is a potential target for transcriptional repression by NFIX. Surprisingly however, the expression of SOX3 within the SCO of $Nfix^{-/-}$ mice was comparable to wild-type mice at E14, E16 and E18 (Fig. 7A and B and data not shown). Normally SOX3 expression by ependymal cells within the SCO is at a lower level than that within ependymal cells lining the walls of the third ventricle (Fig. 6C–F, Fig. 7A'; also see Lee et al., 2012). Sox3 transgenic mice with hydrocephalus exhibit SOX3 expression within the SCO that is comparable to that within cells lining the walls of the third ventricle (Lee et al., 2012). Contrary to our hypothesis, the level of SOX3 expression within the SCO of Nfix mutant mice did not appear elevated in comparison to surrounding tissue (Fig. 7A' and B'), suggesting that upregulation of SOX3 within the SCO of $Nfix^{-/-}$ does not contribute to the formation of hydrocephalus within this line.

2.5. Patterning and function of the SCO is normal in $Nfix^{-/-}$ mice

We next investigated the formation of the SCO in mice lacking Nfix. The SCO develops from neuroepithelial progenitor cells that line the lumen of the dorsal aspect of the diencephalon. The epithelial progenitors of the SCO are driven towards a specialized secretory ependymal cell fate in part via the expression of patterning genes such as Bmp6, which is expressed by the nascent SCO during embryogenesis (Huh et al., 2009; Lee et al., 2012). Analysis of Bmp6 expression via in situ hybridisation during development of the SCO revealed that this gene was expressed by cells within the SCO of both wild-type and Nfix mutant brains at ages between E14 and E18, and that expression levels were comparable between controls and mutants (Fig. 8A–D). Expression of another patterning molecule, Lhx5, was also unchanged in Nfix mutant mice (data not shown). Furthermore, analysis of the development of Reissner's fibre revealed that this structure began to be produced specifically by the ependymal cells of the SCO in both wild-type and mutant brains during late embryogenesis (Fig. 8E–H), and continued to be produced by these cells within the postnatal brain (Fig. 8I and J). Again, we did not detect any qualitative differences in the expression of Reissner's fibre immunoreactivity between wild-type and mutant brains, suggesting that the functionality of the SCO is maintained in the absence of Nfix.

NFIX is part of a larger family of transcription factors that also includes NFIA, NFIB and NFIC, of which the former two have been shown to be strongly expressed within the developing central nervous system (Chaudhry et al., 1997). To ascertain whether other NFI family members may have been compensating for the loss of Nfix, we first analysed the expression of NFIA and NFIB within the developing SCO. Both NFIA and NFIB were expressed by ependymal cells of the SCO during embryogenesis

(Fig. 9A and B). The development of conditional *Nfi* alleles has recently enabled the investigation of consequences of the loss of multiple *Nfi* isoforms in a temporally controlled manner (Hsu et al., 2011; Messina et al., 2010). Using conditional *Nfib* (*Nfib*^Flox/Flox) (Hsu et al., 2011) and *Nfix* (*Nfix*^Flox/Flox) (Messina et al., 2010) alleles we generated a strain containing both *Nfib* and *Nfix* conditional alleles (*Nfib*^Flox/Flox; *Nfix*^Flox/Flox). This was crossed to a Cre deleter strain under which Cre recombinase was under the control of a tamoxifen-inducible ubiquitous Rosa26 promoter (*R26CreER*^T2). The resulting line (*Nfib*^Flox/Flox; *Nfix*^Flox/Flox;

R26CreER^T2) was injected with tamoxifen at E10 and E12 to induce knockout of both *Nfib* and *Nfix*. Analysis of mRNA levels by qPCR revealed that both *Nfib* and *Nfix* levels were reduced by over 90% in comparison to mice that were not carrying the *R26CreER*^T2 allele (data not shown). We then analysed SCO morphology (Fig. 9C–E) as well as SOX3 expression and Reissner's fibre immunoreactivity (Fig. 9F–K) within the SCO of tamoxifen treated *Nfib*^Flox/Flox; *Nfix*^Flox/Flox; *R26CreER*^T2 mice at E18. In spite of the loss of 4 individual alleles, SOX3 expression and Reissner's fibre immunoreactivity was not different from the controls in these mice.

Despite the production of spondin by ependymal cells of the SCO in mice lacking *Nfix*, the possibility of hydrocephalus occurring as a result of stenosis of the Sylvian aqueduct remained a possibility. To address this we analysed hematoxylin-stained coronal sections of P15 wild-type and mutant brains at multiple different rostro-caudal levels. We saw no evidence for stenosis of the aqueduct in *Nfix*^−/− mice (Fig. 10). To investigate this further, we measured the dorso-ventral length of the Sylvian aqueduct at three different levels on coronal sections of P15 wild-type and knockout brains, a measure that has previously been utilised as a proxy for aqueductal stenosis (Nakajima et al., 2011). Again, we saw no significant alterations in this measure of aqueductal morphology between wild-type and knockout brains (Fig. 10G), illustrative of normal aqueduct formation in *Nfix*^−/− mice. Of note, however, was the fact that there was no evidence of dilation within the third ventricle or Sylvian aqueduct of mice lacking *Nfix*, which is in stark contrast to the phenotype within the lateral ventricles of these mice. Moreover, the ependymal cells lining the aqueduct appeared morphologically normal, and we observed no evidence for denudation of this cellular layer within this mutant strain (Fig. 10). This led us to question whether ependymal cells within the lateral ventricles of *Nfix*^−/− mice were normal, as ependymal denudation within the lateral ventricles has previously been implicated in the progression of some models of hydrocephalus (Jimenez et al., 2001).
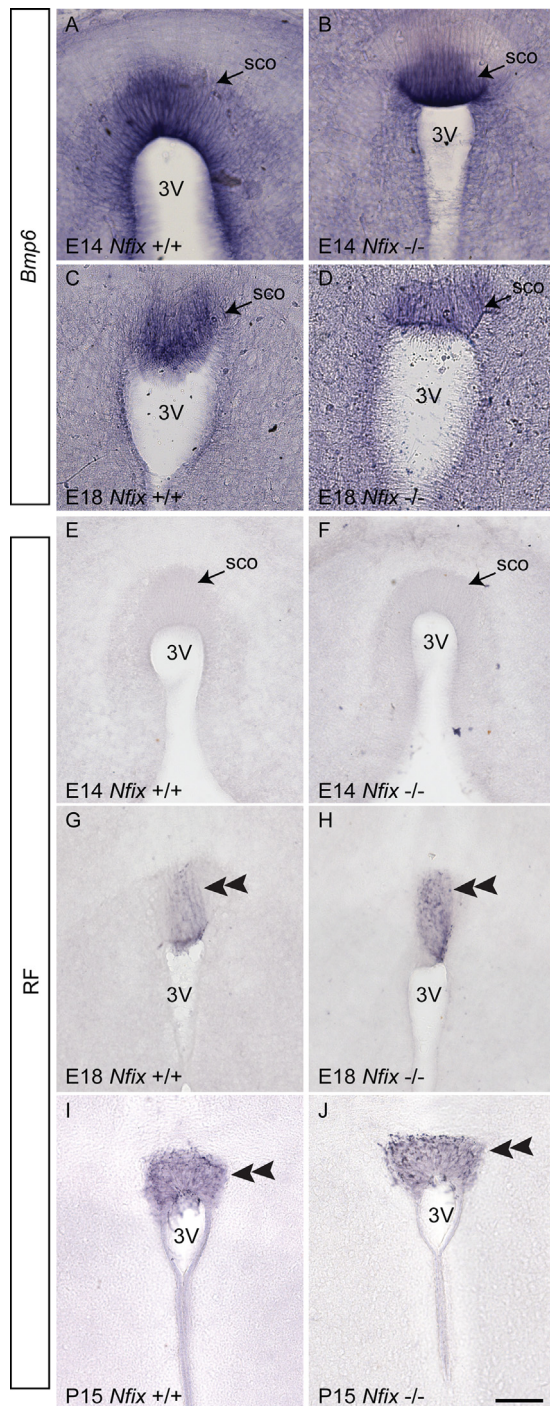

Fig. 8 – Patterning and function of the SCO is not perturbed within *Nfix*^−/− mice. (A–D) Coronal sections of wild-type and *Nfix*^−/− mice showing the expression of *Bmp6* mRNA as revealed by *in situ* hybridisation at E14 (A and B) and E18 (C and D). The expression of *Bmp6* by cells within the SCO was comparable between mutants (B and D) and controls (A and C). (E–J) Coronal sections of E14, E18 and P15 wild-type (E, G, and I) and *Nfix*^−/− (F, H, and J) mice revealing the presence of Reissner's fibre (RF). At E14, RF expression was not detectable within the SCO. By E18, similar levels of expression were evident within the SCO of wild-type and mutant brains (compare double arrowheads in G and H). The presence of RF was also similar between sample groups at P15 (compare double arrowheads in I and J). 3 V = third ventricle. Scale bar (in J): (A, B, E, and F) 50 μm; (C, D, G, and H) 50 μm; (I and J) 75 μm.

2.6. Ependymal cells within the lateral ventricles are abnormal in Nfix$^{-/-}$ mice

Ependymal cells of the lateral ventricles facilitate the flow of CSF via the beating of their cilia that are located within the ventricular lumen (Wilson et al., 2010). The loss of these cells perturbs the flow of CSF and contributes to its build up within the lateral ventricles (Baas et al., 2006). Indeed, a number of mouse models of communicating hydrocephalus have been repor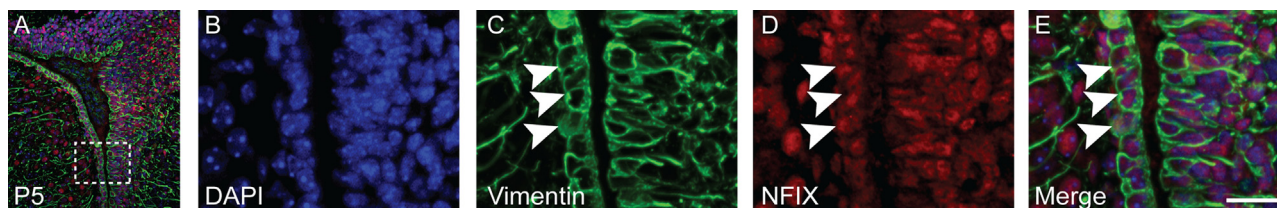ted to display ependymal denudation of the lateral ventricles (Jimenez et al., 2001, 2014), as have hydrocephalic humans (McAllister, 2012). NFIX was recently been shown to be expressed by ependymal cells lining the lateral ventricles of adult mice (Heng et al., in press). We confirmed this, using co-immunofluorescence staining and confocal microscopy to demonstrate that vimentin-expressing ependymal cells also express NFIX at P5 and P10 (Fig. 11 and data not shown). To address the morphology of ependymal cells within the lateral ventricles of Nfix$^{-/-}$ mice, we next examined the expression of vimentin in sections from P5, P10 and P15 wild-type and
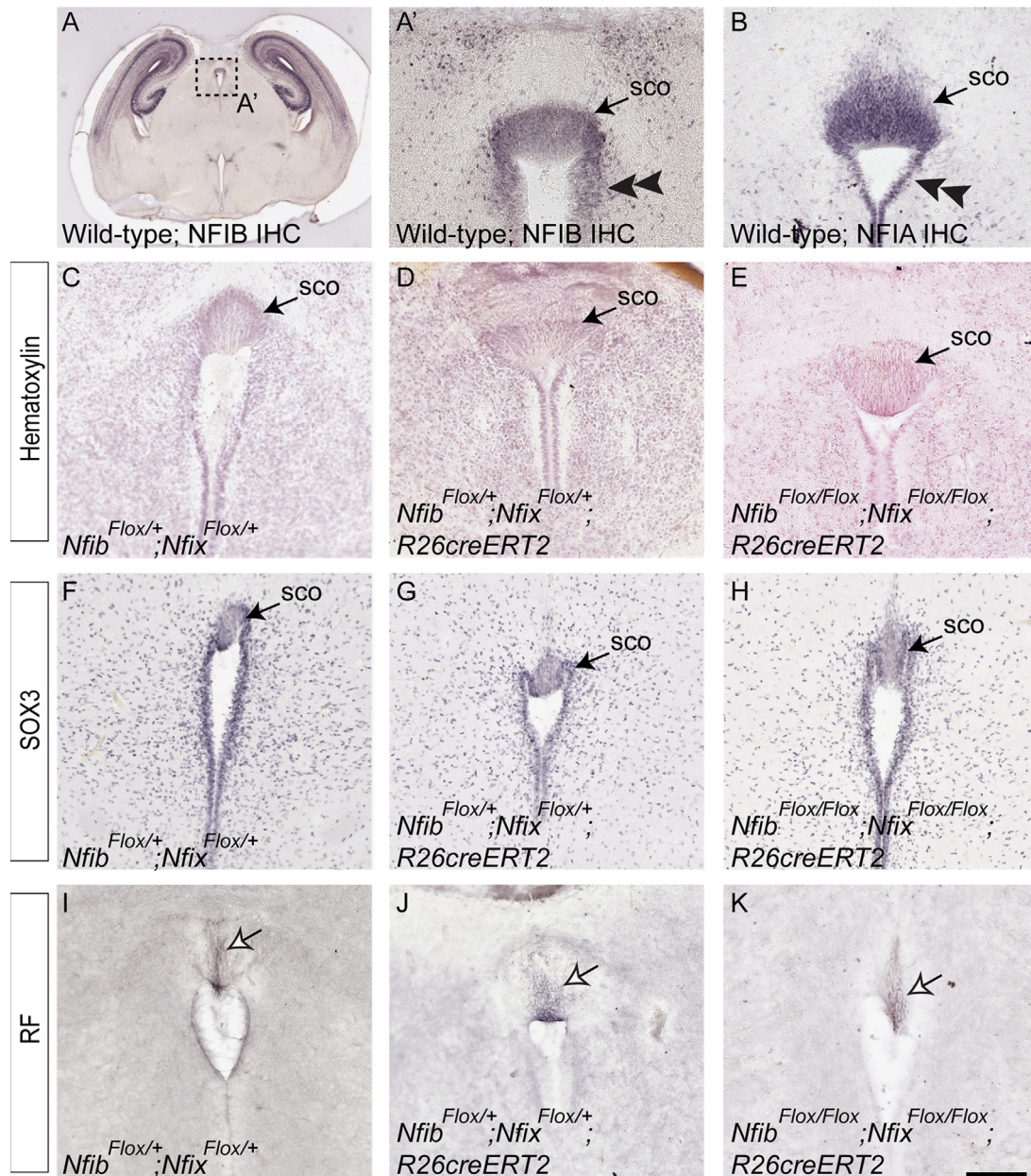
Fig. 9 – The SCO is not functionally perturbed in mice lacking both Nfib and Nfix. (A and B) Coronal sections of E17 wild-type mice, showing the expression of NFIB (A) and NFIA (B). Both of these transcription factors were expressed by ependymal cells within the SCO, as well as by ependymal cells lining the third ventricle (double arrowheads in A', B) at this age. **(C–K)** Coronal sections of E18 control (Nfib$^{Flox/+}$; Nfix$^{Flox/+}$; C, F, and I); double heterozygous Nfi (Nfib$^{Flox/+}$; Nfix$^{Flox/+}$; R26CreER^{T2}; D, G, and J) and double homozygous Nfi (Nfib$^{Flox/Flox}$; Nfix$^{Flox/Flox}$; R26CreER^{T2}; E, H, and K) mice. Hematoxylin staining (C–E) revealed that the SCO appeared morphologically normal in all groups. Similarly, the expression of SOX3 (F–H) and RF (open headed arrows in I–K) was similar across mice from each of these genotypes. Scale bar (in K): (A) 500 μm; (A', and B–K) 50 μm.
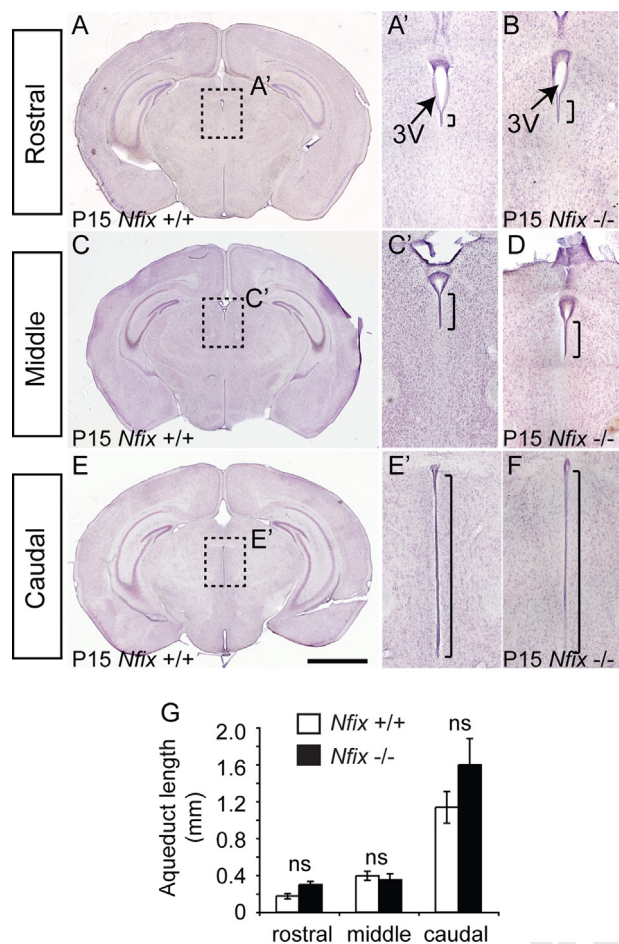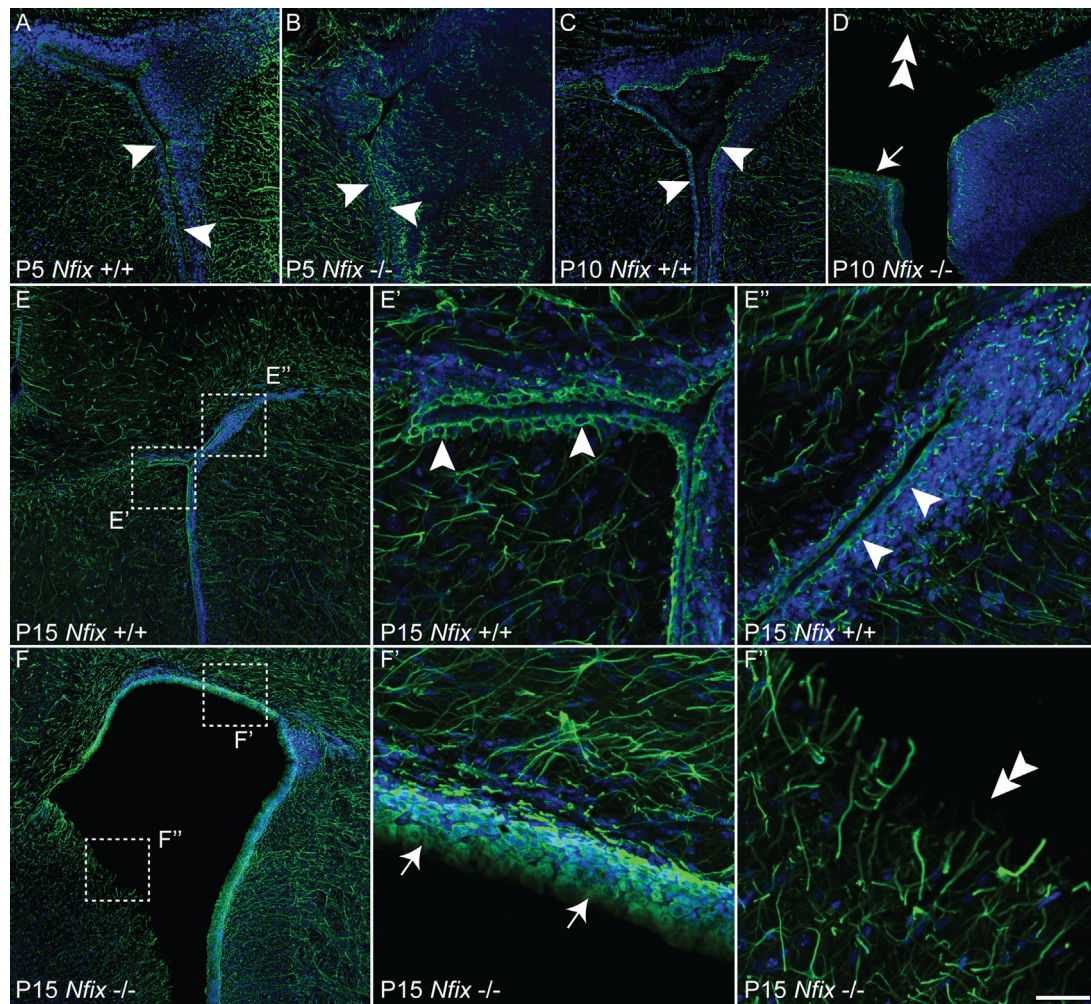
Fig. 10 – $Nfix^{-/-}$ mice do not exhibit aqueductal Stenosis. Coronal sections of P15 wild-type (A, C, and E) and $Nfix^{-/-}$ (B, D, and F) mice stained with hematoxylin. Panels A, C, and E are representative sections from a wild-type mouse that show the position along the rostro-caudal axis that were used to quantify the length of the Sylvian aqueduct. The high power images to the right show the third ventricle (3 V) as well as the length of the Sylvian aqueduct (demarcated by brackets) at rostral (A' and B), middle (C' and D) and caudal (E' and F) levels. There was no significant difference in the length of the aqueduct between genotypes at these positions along the rostro-caudal axis at this age (G; $p > 0.05$, t-test. ns=not significant). Scale bar (in E): (A, C, and E) 600 μm; (A', B, C', D, E' and F) 60 μm.

mutant brains. Within wild-type mice we observed a continuous arrangement of cuboidal, vimentin-expressing lining the lateral ventricles at these ages (Fig. 12A, C and E). In the mutant, however, a number of consistent changes were observed at P10 and P15. Firstly, we frequently observed thickening of the ependymal cell layer, with cells lacking the classical cuboidal shape of normal ependymal cells (Fig. 12D, F, and F'). Secondly, in all of the mice with hydrocephalus that we analysed at P10 and P15 there were regions of the lateral ventricular wall in which the ependymal cells had either failed to develop or had sloughed off completely (Fig. 12D, F, and F''). We also observed this phenotype within postnatal $Nfib^{\pm}$; $Nfix^{\pm}$ mice with hydrocephalus (Fig. 5). Given the crucial role of ependymal cilia on facilitating the flow of CSF (Lee, 2013) our findings indicate that the loss of a functional ependymal cell layer may be the underlying cause of the postnatal hydrocephalus evident within $Nfix^{-/-}$ mice.

We next analysed cellular apoptosis via cleaved caspase 3 immunocytochemistry. We have previously reported that increased apoptosis occurs within the SVZ region of $Nfix^{-/-}$ mice at P10 (Heng et al., in press). We replicated these findings here, demonstrating increased levels of apoptosis within the SVZ of P10 $Nfix^{-/-}$ mice (Suppl. Fig. 2). However, we did not observe any apoptotic cells within the ependymal layer of Nfix mutant mice at either P5 or P10, suggestive of cellular death not playing a direct role in the denudation of the ependyma in these mice. Furthermore, the expression of N-cadherin, a cell-adhesion molecule localised to ependymal cells (Oliver et al., 2013) was not markedly different in $Nfix^{-/-}$ mice at P5 or P10, although the morphology of the ependymal cells expressing this factor was abnormal at P10 (Fig. 13). We also assessed the expression of Celsr2 and Celsr3 mRNAs in tissue isolated from the SVZ of P20 wild-type and $Nfix^{-/-}$ mice using qPCR. These cadherin molecules are known to regulate ependymal ciliogenesis, and mice lacking both of these genes exhibit impaired ciliogenesis and subsequent hydrocephalus (Tissir et al., 2010). However, the expression of these genes was not significantly changed within $Nfix^{-/-}$ mice (data not shown). Furthermore, the expression of acetylated α tubulin, a ciliary component, appeared normal in those regions of the ventricular surface where the ependymal layer was still present within P15 $Nfix^{-/-}$ mice (Suppl. Fig. 3). Finally, we further analysed the ependymal thickening phenotype we observed at P10 and P15 using GFAP immunocytochemistry, as astrocytes have been suggested to

Fig. 11 – NFIX and vimentin are co-expressed by ependymal cells within the lateral ventricles. (A) Coronal sections of a P5 wild-type mice revealing the expression of NFIX (red), vimentin (green) and DAPI (blue) visualised via confocal microscopy (3.0 μm optical sections). The boxed region in A is expanded in panels B–E. Nuclei are shown with DAPI (blue; B). Vimentin expressing ependymal cells (green, C) also express NFIX (red, D), as shown in the merged image (E; arrowheads depict ependymal cells expressing vimentin and NFIX). Scale bar (in E): (A) 100 μm; (C–E) 20 μm. (For interpretation of the references to color in this figure legend, the reader is referred to the web version of this article.)

Fig. 12 – $Nfix^{-/-}$ mice exhibit ependymal denudation within the lateral ventricles. Co-immunofluorescence labelling and confocal microscopy (3.0 μm optical sections) were used to examine the expression of vimentin (green) by cells lining the lateral ventricles of P5, P10 and P15 wild-type (A, C, and E) and $Nfix^{-/-}$ (B, D, and F) mice. In the wild-type, vimentin-expressing ependymal cells were cuboidal in shape, and formed a regular array along the walls of the lateral ventricle (arrowheads in A, C, E' and E''). This was also the case in P5 mutant mice (arrowheads in B). In the mutant at P10 and P15, however, there was frequent thickening of the ependymal layer, and the cells were no longer of a uniform cuboidal shape (arrows in D and F'). Mutant mice also exhibited denudation of the ependymal layer within the lateral ventricles (double arrowhead in D and F''). Nuclei were labelled with DAPI (blue). Scale bar (in F''): (A–F) 100 μm; (E', E'', F', and F'') 20 μm. (For interpretation of the references to color in this figure legend, the reader is referred to the web version of this article.)

assemble at the sites of ependymal denudation to facilitate the re-establishment of the layer separating the CSF and the brain parenchyma (Roales-Buján et al., 2012). Confocal microscopy revealed that the thickened areas within the lateral ventricles of $Nfix^{-/-}$ mice were strongly immunoreactive for GFAP, suggestive of these zones being the sites of astroglial scarring in response to ependymal denudation (Fig. 14).

3. Discussion

Hydrocephalus is a relatively common birth defect (Bruni et al., 1985) but despite its prevalence, and the existence of several rodent models of this disorder (Jones and Bucknall, 1988; Lee et al., 2012; Perez-Figares et al., 1998), our understanding of the molecular and cellular mechanisms leading to the pathological CSF accumulation remains limited. Here we reveal that hydrocephalus is a consistent feature present in mice lacking the transcription factor Nfix, implicating normal NFIX function as being central to the formation of the intraventricular region of the central nervous system. Specifically, we demonstrated that NFIX is central to the biology of ependymal cells, and that, in its absence, the lateral ventricles of the dorsal telencephalon exhibit denudation of the ependymal cell layer.

Ependymal cells lining the walls of the brain ventricles are post-mitotic cells that are derived from radial glial progenitors during embryonic development (Spassky et al., 2005). NFI family members, including NFIX, have previously been shown to be expressed by radial glia within the dorsal telencephalon (Campbell et al., 2008; Plachez et al., 2008). Moreover, a number of recent studies have begun to elucidate
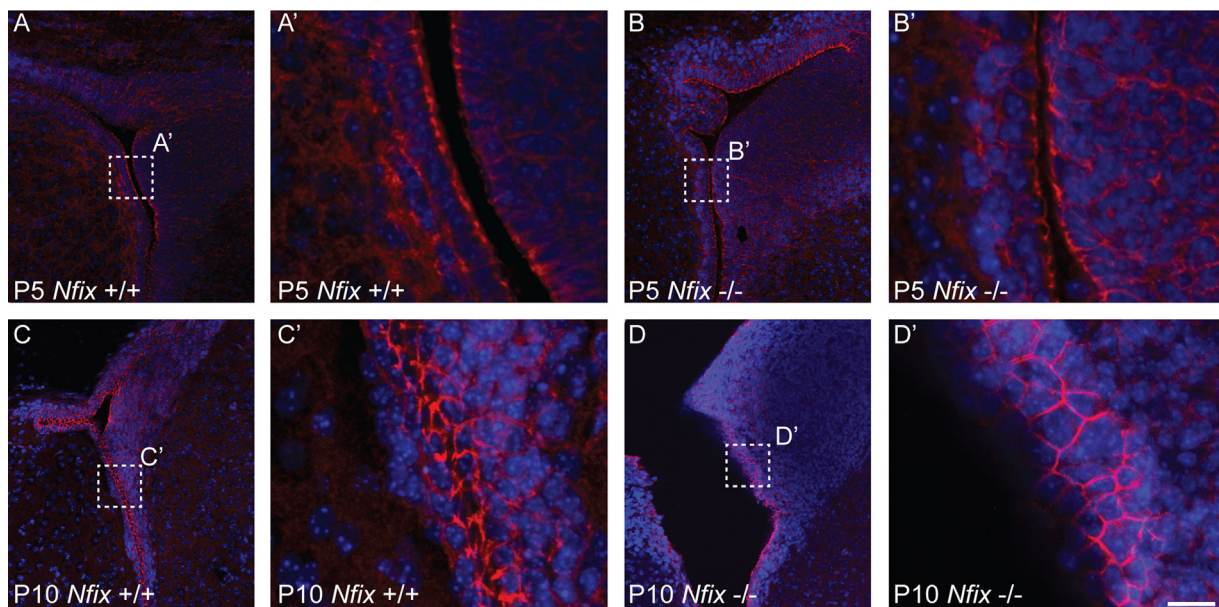
Fig. 13 – N-cadherin is expressed by ependymal cells of the lateral ventricles in $Nfix^{-/-}$ mice. Coronal sections of P5 and P10 wild-type (A and C) and mutant (B and D) mice showing the expression of DAPI (blue) and N-cadherin (red). This adhesion molecule is expressed on the surface of ependymal cells in both the wild-type (A' and C') and the mutant (B' and D') mice at these ages. Scale bar (in D'): (A–D) 100 μm; (A'–D') 20 μm. (For interpretation of the references to color in this figure legend, the reader is referred to the web version of this article.)
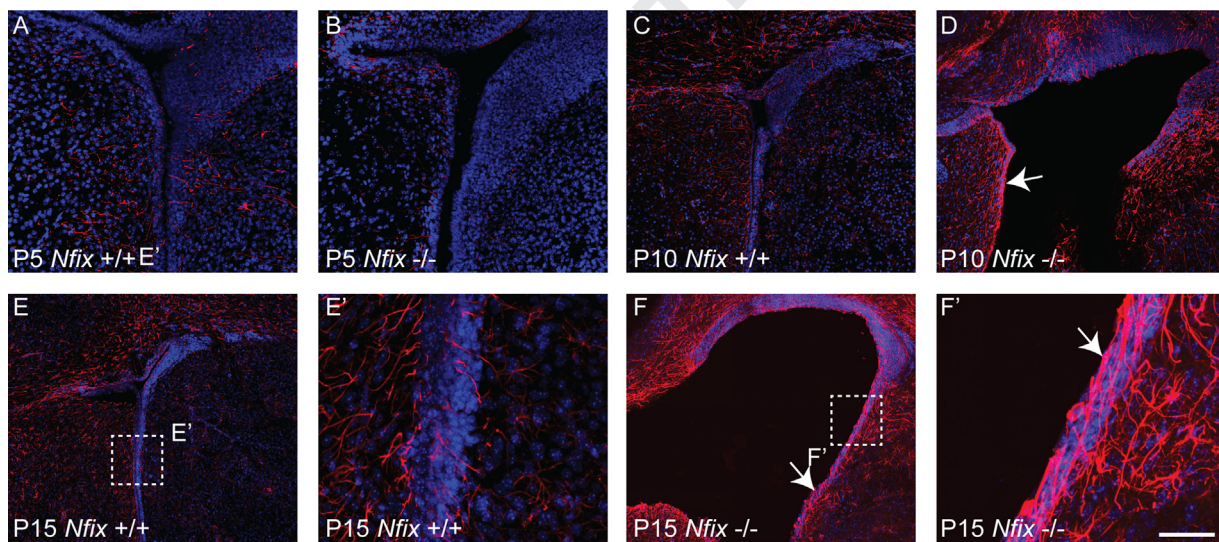
Fig. 14 – Aberrant expression of GFAP within the thickened ependyma of $Nfix^{-/-}$ mice. Coronal sections of P5, P10 and P15 wild-type (A, C, and E) and mutant (B, D, and F) mice showing the expression of DAPI (blue) and GFAP (red). At P5, the expression of GFAP is comparable between wild-type and mutant mice (A and B). At P10, however, GFAP expression is elevated in regions of the lateral ventricles that appear thickened in the mutant (arrow in D), a phenotype also seen at P15 (arrows in F and F'). Scale bar (in F'): (A–F), 100 μm; (E' and F') 20 μm. (For interpretation of the references to color in this figure legend, the reader is referred to the web version of this article.)

the role of NFI proteins within ventricular zone neural progenitor cells (Harris et al., 2014), revealing that NFIs mediate radial glia differentiation in a number of distinct ways, including via the repression of pathways mediating progenitor cell self-renewal (Heng et al., 2014a; Piper et al., 2014), through the activation of differentiation-specific genetic programmes (Cebolla and Vallejo, 2006), and by indirectly influencing epigenetic DNA methylation of target genes such as *glial fibrillary acidic protein* (Namihira et al., 2009). These reports demonstrate a central role of NFI proteins in mediating the differentiation of radial glia during development.

Studies have also shown that NFIA, NFIB and NFIX are also expressed by ependymal cells lining the ventricles of the brain in both postnatal and adult mice (Campbell et al., 2008; Plachez et al., 2008). Given the reports of hydrocephalus in

Nfix^{-/-} mice (Campbell et al., 2008; Driller et al., 2007), this led us to hypothesise that NFIX may be mediating the formation and/or function of the SCO, a specialized ependymal gland located at the roof of the third ventricle (Huh et al., 2009). There were a number of lines of evidence that led us to this hypothesis. Firstly, the Sylvian aqueduct is the most common cause of intraventricular blockage in cases of hydrocephalus (Cinalli et al., 2011), and normal SCO development and function is central to maintaining the patency of this aqueduct (Huh et al., 2009; Perez-Figares et al., 2001). Secondly, NFIX has recently been shown to repress members of the Sox family of transcription factors, including Sox9 and Bbx (Dixon et al., 2013; Heng et al., 2014a). Moreover, we also reported that Sox3 is upregulated within the hippocampus of mice lacking Nfix at E16 (Heng et al., 2014a). When considered in light of a recent report demonstrating that overexpression of SOX3 within the SCO culminates in hydrocephalus (Lee et al., 2012), we postulated that upregulation of SOX3 within the SCO of mice lacking Nfix may underlie the hydrocephalic phenotype of these mice.

Contrary to our hypothesis, the development of the SCO in Nfix^{-/-} mice was morphologically normal, with no evidence for upregulation of SOX3 within the ependymal cells of this organ. Moreover, Reissner's fibre was produced within the SCO of Nfix mutant mice in a manner similar to that of wild-type mice. Finally, we found no evidence for aqueductal stenosis in this mutant strain, illustrative of other factors contributing to the hydrocephalus evident within these mice. Do these findings suggest that NFI proteins do not contribute to the formation and/or function of the SCO? At this stage, it is unclear whether NFI function is redundant for development of the SCO. Importantly, embryonic expression of both SOX3 and spondin was normal in Nfib[Flox/Flox]; Nfix[Flox/Flox]; R26CreER[T2] mice, suggesting that the loss of 4 Nfi alleles is not sufficient to perturb SCO development. However, NFIA is also strongly expressed by the developing SCO, suggesting that its presence may be sufficient to compensate to the loss of both Nfib and Nfix. Moreover, these double mutants die at birth, precluding postnatal investigation of whether these mice develop hydrocephalus in a fashion akin to Nfix mutant mice. Future experiments centred on the conditional ablation of all three of these genes specifically from cells within the SCO are required to determine whether or not NFIs are dispensable for the genesis and the function of this organ.

Instead, the main phenotype exhibited by Nfix mutant mice was denudation of the ependymal layer of the lateral ventricles. Although we cannot definitively ascertain whether this is the cause of hydrocephalus in these mice, or a consequence of raised intraventricular pressure, recent reports from the literature suggest that the loss of ependymal cells may indeed underlie the development of hydrocephalus in both rodent models of this disorder and within human patients (Dominguez-Pinos et al., 2005; Jimenez et al., 2014). For instance, ependymal cell denudation is one of the prominent features in the hyh (hydrocephalus with hop gait) mouse (Paez et al., 2007). These mice, which carry mutations to the alpha-SNAP gene (Chae et al., 2004), exhibit aqueducal stenosis due to absence of the neuroepithelium/ependymal cell layer (Wagner et al., 2003). Crucially, however, neuroepithelial/ependymal denudation in hyh mice occurs embryonically, prior to the development of hydrocephalus (Jimenez et al., 2001), suggestive of primary

deficits in the ependymal cell layer as being the causative agents of postnatal hydrocephalus within this mutant strain. Conditional ablation of the Ras-related GTPase Cdc42 also culminates in ependymal cell denudation and hydrocephalus (Peng et al., 2013), further underlining the importance of ependymal cells in the development of this disorder.

Abnormal subcellular distribution of the cell adhesion molecule, N-cadherin, has also been linked to ependymal cell denudation within another human disorder, namely spina bifida aperta (Sival et al., 2011). N-cadherin constitutes part of the adherens junction within neuroepithelial/ependymal cells, and is thus postulated to regulate the stability of this cellular layer (Jimenez et al., 2014). With regards to hydrocephalus, disruption of N-cadherin based adherens junctions within an in vitro organotypic model of bovine ventricular ependymal cell development was recently shown to lead to the disruption of ependymal cell adherens junctions, and to culminate in apoptosis of the ependymal cell layer (Oliver et al., 2013). Within this in vitro model there are no extrinsic mechanical factors present, such as elevated ventricular pressure, suggesting that ependymal cell denudation can occur in isolation from increased ventricular pressure, and further implicate N-cadherin-mediated adherens junctions as being pivotal for normal ependymal cell biology. Could the phenotype within Nfix^{-/-} mice be related to abnormal N-cadherin expression? Interestingly, we identified a putative NFI binding site in the upstream region of the N-cadherin (Cdh2) promoter (Table 1), suggestive of potential regulation of N-cadherin expression by NFI family members. However, the expression levels of N-cadherin within the ependyma of Nfix^{-/-} mice at P10 were not noticeably different from that seen in wild-type controls (Fig. 13). Moreover, although we identified NFI binding sites within other genes involved in the development of ependymal cell polarity, including Celsr2 and Celsr3 (Table 1), the expression of these factors was not significantly different within tissue isolated from the SVZ of P20 mutant mice. At this stage, however, it is too early to rule out abnormal expression and/or sub-cellular localisation of these factors as contributing factors to the hydrocephalus evident within Nfix^{-/-} mice. Future studies based upon gene expression profiling (single cell mRNA profiling on ependymal cells isolated from wild-type and mutant brains) and sub-cellular investigation of protein localisation are required to determine whether abnormal adhesion and polarity are important facets that contribute to hydrocephalus within Nfix^{-/-} mice. In addition, the analysis of ciliary morphology, perhaps through scanning electron microscopy, will be critical to perform, as impaired ciliogenesis is implicated in hydrocephalus (Lattke et al., 2012).

Our work also revealed that an astroglial scar formed in some areas of the ventricular wall of Nfix^{-/-} mice (Fig. 14). This is in accordance with other instances of ependymal cell denudation, such as that seen in the hyh mouse, where periventricular astrocytes expand to form a new cellular layer over the denuded ventricular surface (Roales-Bujan et al., 2012). This suggests that some compensatory mechanisms exist to drive gliogenesis within these periventricular astrocytes, although the cellular and molecular mechanisms underpinning this also remain undefined at this stage.

One final question that arises is why the ependyma of the lateral ventricles is affected in our mutant mice, yet the

Table 2 – Primary antibodies used in this study. The source, dilution and use (Immunohistochemistry – IHC, or immunofluorescence – IF) of the antibodies used in this study are given below.

Antibody	Host	Source	Use	Dilution
NFIX	Rabbit polyclonal	Abcam, ab101341	IHC	1/1000
NFIX	Mouse monoclonal	Sigma-Aldrich, SAB1401263	IF	1/400
SOX3	Goat polyclonal	R&D Biosciences, AF2569	IHC	1/5000
SOX3	Goat polyclonal	R&D Biosciences, AF2569	IF	1/100
Vimentin	Rabbit monoclonal	Abcam, ab92547	IF	1/500
RF	Rabbit polyclonal	Gift from Dr. A Meiniel	IHC	1/50,000
GFAP	Rabbit polyclonal	Dako, Z0334	IF	1/1000
N-cadherin	Mouse monoclonal	BD Biosciences, 610,920	IF	1/200
Cleaved caspase 3	Rabbit polyclonal	Cell Signalling Technology, 9661	IF	1/200
Acetylated α tubulin	Mouse monoclonal	Sigma, T7451	IF	1/2000

ependyma of the third ventricle is not? Currently this remains an open question, though we speculate that multiple causes could underlie these phenomena. For instance, the NFI family seem to play a critical role in the development of the dorsal telencephalon, with dramatic phenotypes evident within the cerebral cortex of Nfia (Piper et al., 2010), Nfib (Barry et al., 2008) and Nfix (Heng et al., in press) knockout mice. However, these knockout strains do not present with such drastic phenotypes within other regions of the brain, despite the strong expression of NFI isoforms by progenitor cells within the ventricular zone throughout the neuraxis (Campbell et al., 2008; Plachez et al., 2008). This is perhaps indicative of compensatory mechanisms working to spare the ependyma of the rest of the ventricular system. Alternatively, one of the most dramatic phenotypes evident within the SVZ/lateral ventricular region of $Nfix^{-/-}$ mice is the marked expansion of the SVZ (Heng et al., in press), a phenotype unique to this region of the mutant brain. One could speculate that the buildup of cells within this region, and the apoptosis that accompanies it, may culminate in altered cellular dynamics that place more stress on the ependymal cells within this region, leading to ependymal denudation. Further studies are required to address this question fully. In conclusion, our findings illustrate that the hydrocephalus evident within $Nfix^{-/-}$ mice (Campbell et al., 2008; Driller et al., 2007) arises not from abnormal development of the SCO or from aqueductal stenosis, but rather from denudation of the ependymal layer of the lateral ventricles, providing a further context in which NFIX function is critical for the normal development and function of the central nervous system.

4. Materials and methods

4.1. Animals and genotyping

$Nfix^{-/-}$ and $Nfix^{+/+}$ littermate mice were used in this study. These mice were maintained on a C57Bl/6 background. They were bred at the University of Queensland under approval from the Institutional Animal Ethics Committee. Timed-pregnant females were obtained by placing $Nfix^{\pm}$ male and female mice together overnight. If the female had a vaginal plug the following day it was designated as E0. The genotype of each mouse was confirmed by polymerase chain reaction (PCR) on DNA prepared from toe samples. The primers used in the reaction amplified a 213 base pair DNA band corresponding to the wild-type Nfix allele or a 309 base-pair DNA band corresponding to the Nfix null allele (Campbell et al., 2008). $Nfib^{\pm}$; $Nfix^{\pm}$ mice were also used in this study, and were bred at the State University of Buffalo under approval from the Institutional Animal Care and Use Committee. The Nfib null allele was identified using PCR as described previously (Steele-Perkins et al., 2005). $Nfib^{Flox/Flox}$ and $Nfix^{Flox/Flox}$ mice were also used in this study (Hsu et al., 2011; Messina et al., 2010), and were also bred at the State University of Buffalo under approval from the Institutional Animal Care and Use Committee. These mice were also genotyped using PCR and sequences of the primers are available upon request.

4.2. Preparation of tissue

Brains were collected at embryonic day (E) 14, E16, E18, P2, P10, P5, P10, P15, P20 and P37. E14 brains were dropped fixed in 4% paraformaldehyde (PFA) in phosphate buffered saline (PBS). From E16 onwards mice were perfused with PBS followed by 4% PFA. Brains were post-fixed in 4% PFA at 4 °C until required. Brains were removed from the skull, embedded in 3% noble agar (Difco Sparks, MD USA) and 50 μm coronal or sagittal sections were cut using a vibratome (Lecia, Nussloch Germany).

4.3. Haematoxylin staining

Tissue sections were mounted and dried on Superfrost Plus slides before being incubated Mayer's hematoxylin (Sigma-Aldrich solution) for 3 min. The slides were then washed with water before being dehydrated in an ethanol–xylene series and cover-slipped using the mounting medium DPX.

4.4. Immunohistochemistry

Immunohistochemistry on floating tissue sections was performed as described previously (Barry et al., 2008) using the chromogen 3,3'-diaminobenzidine (DAB). Briefly, sections were incubated overnight with the primary antibody, and then incubated for 1 h with biotinylated secondary antibodies. Antibody details and the dilution at which they were used are listed in Table 2. Sections were then incubated for 1 h in avidin–biotin complex (Vectastain ABC kit; Vector Laboratories) before being

incubated in the colour reaction solution (nickel-DAB chromogen solution activated with 0.01% v/v hydrogen peroxide). The colour reaction was terminated by rinsing sections in PBS. Following staining, tissue sections were mounted onto gelatinized Superfrost slides before being dehydrated in an ethanol-xylene series and cover-slipped using DPX. Immunohistochemistry on paraffin sections was performed as above, with the additional inclusion of an antigen retrieval step (boiling citrate treatment, pH 6.0) as described previously (Piper et al., 2010).

4.5. Immunofluorescence

To perform co-immunofluorescence labelling, sections were processed for antigen retrieval (sodium citrate buffer, pH 6.0, 95 °C, 15 min, before being incubated overnight with the primary antibodies at 4 °C. They were then washed and incubated in a solution containing the secondary antibodies, before being washed again and counterstained with 4′,6-diamidino-2-phenylindole (DAPI). The secondary antibodies used in this study were goat anti-rabbit IgG AlexaFluor488 (Invitrogen; 1/250), goat anti-rabbit IgG AlexaFluor568 (Invitrogen; 1/250), goat anti-mouse IgG AlexaFluor 647 (Invitrogen; 1/250) and goat anti-mouse IgG AlexaFluor488 (Invitrogen; 1/250). The secondary antibody used to detect the SOX3 primary antibody was biotin-conjugated rabbit anti-goat IgG (1/1000; Vector Laboratories) followed by incubation with Streptavidin-Cy3 (1/250; Invitrogen). Sections were then mounted in fluorescent mounting medium (DAKO). Sections labelled with fluorescent antibodies were imaged with a Zeiss Axio Observer Z1 spinning disk confocal using Slidebook software (3i). The data presented are from three adjacent merged 1.0 μm confocal z-stacks of the stained tissue.

4.6. In situ hybridisation

Mouse brains were collected at embryonic E14, E16 and E18 and fixed and sectioned as described above. Brain sections were mounted onto Superfrost plus slides (Menzel-Glaser, Brunswick, Germany) (n=5 for both wild type and knockout mice), air dried for one hour then processed for in situ hybridisation. In situ hybridisation was performed as described previously (Piper et al., 2009), with minor modifications. Antisense riboprobes against Lhx5 and Bmp6 were used in this study. The hybridisation temperature was 68 °C, and the colour reaction was performed using the substrate BM Purple (Roche). Slides were then coverslipped with Hydromount (National Diagnostics).

4.7. Image acquisition and analysis

Sections were imaged for bright-field microscopy using an upright microscope (Zeiss Z1, Zeiss, Goettingen, Germany) attached to a digital camera (Zeiss AxioCam HRc) using AxioVision software (Zeiss). Sections labelled with fluorescent antibodies were imaged with a Zeiss Axio Observer Z1 spinning disk confocal using Slidebook software (3i). The data presented are from three adjacent merged 1.0 μm confocal z-stacks of the stained tissue. When comparing wild-type to knockout tissue, sections from matching positions along the rostro-caudal axis were selected. For all experiments, sections from n>5 different

brains of each genotype were analysed. Quantification of ventricular area, total brain area and aqueduct length was performed using the freeware programme ImageJ. To perform cell counts of SOX3-positive cells within the neocortical and hippocampal ventricular zone, the total number of immuno-positive cells per 100 μm was counted. Two independent 100 μm regions were counted for each neocortical or hippocampal section. For all experiments involving quantification, data represent pooled results from at least 5 wild-type and 5 Nfix$^{-/-}$ brains. Quantification was performed blind to the genotype of the sample, and statistical analyses were performed using a 2-tailed unpaired t-test. Error bars represent the standard error of the mean.

4.8. Bioinformatic promoter screen

The NFI binding motif was generated as reported previously (Heng et al., 2014a) from published chromatin immunoprecipitation-sequencing (ChIP-seq) data for NFI (pan-NFI antibody used) (Pjanic et al., 2011). Potential NFI binding sites promoter was identified using the MEME algorithm and the FIMO motif-scanning programme as described previously. FIMO was run on the mouse genome (without repeat masking) using a 0-order background generated on the entire mouse genome, and a pseudocount of 0.1. All potential binding sites with p-value $\leq 10^{-4}$ were reported in the region of -3000 base pairs to $+200$ base pairs relative to the transcription start site (TSS) of relevant genes. Putative NFI binding sites near the Sox3 promoter were identified by viewing the FIMO output using the UCSC genome browser (Table 1).

4.9. Luciferase reporter assay

Our bioinformatic promoter screen identified six potential NFI binding sites within the Sox3 promoter, with four of these being within 2000 base pairs of the transcription start site (TSS), namely at -27 base pairs relative to the TSS (chromosome X: 58146618-58146632, CGGGAAGCCTGCCCG), -471 base pairs relative to the TSS (chromosome X: 58147062-58147076, CTGGAAAGCTCCCCG), -745 base pairs relative to the TSS (chromosome X: 58147336-58147350, TGGGGGGGTTTGCCAG) and -1237 base pairs relative to the TSS (chromosome X: 58147828-58147842, TGGGTTATCTGCCAA). An expression vector containing the full length Nfix gene driven by the chick β-actin promoter (Nfix pCAGIG), and a luciferase reporter construct containing a 1278 base pair fragment of the mouse Sox3 promoter sequence (containing these 4 putative NFI binding sites, chromosome X: 58146604-58147882) cloned upstream of the Renilla luciferase gene (pLightSwitch Sox3; this construct was obtained from Switchgear Genomics) were used for the luciferase assays. NSC34 cells were seeded at 1×10^{5} cells per well of a 96 well plate 24 h prior to transfection. DNA was transfected into cells using FuGENE (Invitrogen). Cypridina luciferase was added to each transfection as a normalisation control. After 24 h, luciferase activity was measured using a dual luciferase system (Switchgear Genomics). Within each experiment, each treatment was replicated three times. Each experiment was also independently replicated a minimum of three times. These experiments were also replicated using a second cell line, Neuro2A. Statistical analyses were performed

using an ANOVA. Error bars indicate the standard error of the mean.

Appendix A.   Supporting information

Supplementary data associated with this article can be found in the online version at http://dx.doi.org/10.1016/j.brainres.2015.04.057.

REFERENCES

Baas, D., Meiniel, A., Benadiba, C., Bonnafe, E., Meiniel, O., Reith, W., Durand, B., 2006. A deficiency in RFX3 causes hydrocephalus associated with abnormal differentiation of ependymal cells. Eur. J. Neurosci. 24, 1020–1030.

Barry, G., Piper, M., Lindwall, C., Moldrich, R., Mason, S., Little, E., Sarkar, A., Tole, S., Gronostajski, R.M., Richards, L.J., 2008. Specific glial populations regulate hippocampal morphogenesis. J. Neurosci. 28, 12328–12340.

Blackshear, P.J., Graves, J.P., Stumpo, D.J., Cobos, I., Rubenstein, J. L., Zeldin, D.C., 2003. Graded phenotypic response to partial and complete deficiency of a brain-specific transcript variant of the winged helix transcription factor RFX4. Development 130, 4539–4552.

Bruni, J.E., Del Bigio, M.R., Clattenburg, R.E., 1985. Ependyma: normal and pathological. A review of the literature. Brain Res. 356, 1–19.

Campbell, C.E., Piper, M., Plachez, C., Yeh, Y.T., Baizer, J.S., Osinski, J.M., Litwack, E.D., Richards, L.J., Gronostajski, R.M., 2008. The transcription factor Nfix is essential for normal brain development. BMC Dev. Biol., 8.

Cebolla, B., Vallejo, M., 2006. Nuclear factor-I regulates glial fibrillary acidic protein gene expression in astrocytes differentiated from cortical precursor cells. J. Neurochem. 97, 1057–1070.

Chae, T.H., Kim, S., Marz, K.E., Hanson, P.I., Walsh, C.A., 2004. The hyh mutation uncovers roles for alpha Snap in apical protein localization and control of neural cell fate. Nat. Genet. 36, 264–270.

Chaudhry, A.Z., Lyons, G.E., Gronostajski, R.M., 1997. Expression patterns of the four nuclear factor I genes during mouse embryogenesis indicate a potential role in development. Dev. Dyn. 208, 313–325.

Cinalli, G., Spennato, P., Nastro, A., Aliberti, F., Trischitta, V., Ruggiero, C., Mirone, G., Cianciulli, E., 2011. Hydrocephalus in aqueductal stenosis. Childs Nerv. Syst. 27, 1621–1642.

Creveaux, I., Gobron, S., Meiniel, R., Dastugue, B., Meiniel, A., 1998. Complex expression pattern of the SCO-spondin gene in the bovine subcommissural organ: toward an explanation for Reissner's fiber complexity. Brain Res. Mol. Brain Res. 55, 45–53.

Del Bigio, M.R., 2010. Ependymal cells: biology and pathology. Acta Neuropathol. 119, 55–73.

Dietrich, P., Shanmugasundaram, R., Shuyu, E., Dragatsis, I., 2009. Congenital hydrocephalus associated with abnormal subcommissural organ in mice lacking huntingtin in Wnt1 cell lineages. Hum. Mol. Genet. 18, 142–150.

Dixon, C., Harvey, T.J., Smith, A.G., Gronostajski, R.M., Bailey, T.L., Piper, M., 2013. Nuclear factor one X regulates bobby sox during development of the mouse forebrain. Cell Mol. Neurobiol. 33, 867–873.

Dominguez-Pinos, M.D., Paez, P., Jimenez, A.J., Weil, B., Arraez, M.A., Perez-Figares, J.M., Rodriguez, E.M., 2005. Ependymal denudation and alterations of the subventricular zone occur in human fetuses with a moderate communicating hydrocephalus. J. Neuropathol. Exp. Neurol. 64, 595–604.

Driller, K., Pagenstecher, A., Uhl, M., Omran, H., Berlis, A., Grunder, A., Sippel, A.E., 2007. Nuclear factor I X deficiency causes brain malformation and severe skeletal defects. Mol. Cell Biol. 27, 3855–3867.

Harris, L., Dixon, C., Cato, K., Heng, Y.H., Kurniawan, N.D., Ullmann, J.F., Janke, A.L., Gronostajski, R.M., Richards, L.J., Burne, T.H., Piper, M., 2013. Heterozygosity for nuclear factor one X affects hippocampal-dependent behaviour in mice. PLoS One 8, e65478.

Harris, L., Genovesi, L.A., Gronostajski, R.M., Wainwright, B.J., Piper, M., 2014. Nuclear factor one transcription factors: divergent functions in developmental versus adult stem cell populations. Dev. Dyn. 3, 227–238.

Heng, Y.H., Barry, G., Richards, L.J., Piper, M., 2012. Nuclear factor I genes regulate neuronal migration. Neurosignals 20, 159–167.

Heng, Y.H., McLeay, R.C., Harvey, T.J., Smith, A.G., Barry, G., Cato, K., Plachez, C., Little, E., Mason, S., Dixon, C., Gronostajski, R. M., Bailey, T.L., Richards, L.J., Piper, M., 2014a. NFIX regulates neural progenitor cell differentiation during hippocampal morphogenesis. Cereb. Cortex 24, 261–279.

Heng, Y.H., Zhou, B., Harris, L., Harvey, T., Smith, A., Horne, E., Martynoga, B., Andersen, J., Achimastou, A., Cato, K., Richards, L.J., Gronostajski, R.M., Yeo, G.S., Guillemot, F., Bailey, T.L., Piper, M., 2015. NFIX regulates proliferation and migration within the murine SVZ neurogenic niche. Cereb. Cortex, http://dxdoi.org/10.1093/cercor/bhu253 (in press).

Hsu, Y.C., Osinski, J., Campbell, C.E., Litwack, E.D., Wang, D., Liu, S., Bachurski, C.J., Gronostajski, R.M., 2011. Mesenchymal nuclear factor I B regulates cell proliferation and epithelial differentiation during lung maturation. Dev. Biol. 354, 242–252.

Huh, M.S., Todd, M.A., Picketts, D.J., 2009. SCO-ping out the mechanisms underlying the etiology of hydrocephalus. Physiology 24, 117–126.

Jimenez, A.J., Tome, M., Paez, P., Wagner, C., Rodriguez, S., Fernandez-Llebrez, P., Rodriguez, E.M., Perez-Figares, J.M., 2001. A programmed ependymal denudation precedes congenital hydrocephalus in the hyh mutant mouse. J. Neuropathol. Exp. Neurol. 60, 1105–1119.

Jimenez, A.J., Dominguez-Pinos, M.D., Guerra, M.M., Fernandez-Llebrez, P., Perez-Figares, J.M., 2014. Structure and function of the ependymal barrier and diseases associated with ependyma disruption. Tissue Barriers 2, e28426.

Jones, H.C., Bucknall, R.M., 1988. Inherited prenatal hydrocephalus in the H-Tx rat: a morphological study. Neuropathol. Appl. Neurobiol. 14, 263–274.

Lattke, M., Magnutzki, A., Walther, P., Wirth, T., Baumann, B., 2012. Nuclear factor kappaB activation impairs ependymal

ciliogenesis and links neuroinflammation to hydrocephalus formation. J. Neurosci. 32, 11511–11523.

Lee, K., Tan, J., Morris, M.B., Rizzoti, K., Hughes, J., Cheah, P.S., Felquer, F., Liu, X., Piltz, S., Lovell-Badge, R., Thomas, P.Q., 2012. Congenital hydrocephalus and abnormal subcommissural organ development in Sox3 transgenic mice. PLoS One 7, e29041.

Lee, L., 2013. Riding the wave of ependymal cilia: genetic susceptibility to hydrocephalus in primary ciliary dyskinesia. J. Neurosci. Res. 91, 1117–1132.

Louvi, A., Wassef, M., 2000. Ectopic engrailed 1 expression in the dorsal midline causes cell death, abnormal differentiation of circumventricular organs and errors in axonal pathfinding. Development 127, 4061–4071.

Mason, S., Piper, M., Gronostajski, R.M., Richards, L.J., 2009. Nuclear factor one transcription factors in CNS development. Mol. Neurobiol. 39, 10–23.

McAllister 2nd, J.P., 2012. Pathophysiology of congenital and neonatal hydrocephalus. Semin. Fetal Neonatal Med. 17, 285–294.

Messina, G., Biressi, S., Monteverde, S., Magli, A., Cassano, M., Perani, L., Roncaglia, E., Tagliafico, E., Starnes, L., Campbell, C.E., Grossi, M., Goldhamer, D.J., Gronostajski, R.M., Cossu, G., 2010. Nfix regulates fetal-specific transcription in developing skeletal muscle. Cell 140, 554–566.

Nakajima, M., Matsuda, K., Miyauchi, N., Fukunaga, Y., Watanabe, S., Okuyama, S., Perez, J., Fernandez-Llebrez, P., Shen, J., Furukawa, Y., 2011. Hydrocephalus and abnormal subcommissural organ in mice lacking presenilin-1 in Wnt1 cell lineages. Brain Res. 1382, 275–281.

Namihira, M., Kohyama, J., Semi, K., Sanosaka, T., Deneen, B., Taga, T., Nakashima, K., 2009. Committed neuronal precursors confer astrocytic potential on residual neural precursor cells. Dev. Cell 16, 245–255.

Oliver, C., Gonzalez, C.A., Alvial, G., Flores, C.A., Rodriguez, E.M., Batiz, L.F., 2013. Disruption of CDH2/N-cadherin-based adherens junctions leads to apoptosis of ependymal cells and denudation of brain ventricular walls. J. Neuropathol. Exp. Neurol. 72, 846–860.

Paez, P., Batiz, L.F., Roales-Bujan, R., Rodriguez-Perez, L.M., Rodriguez, S., Jimenez, A.J., Rodriguez, E.M., Perez-Figares, J.M., 2007. Patterned neuropathologic events occurring in hyh congenital hydrocephalic mutant mice. J. Neuropathol. Exp. Neurol. 66, 1082–1092.

Peng, X., Lin, Q., Liu, Y., Jin, Y., Druso, J.E., Antonyak, M.A., Guan, J.L., Cerione, R.A., 2013. Inactivation of Cdc42 in embryonic brain results in hydrocephalus with ependymal cell defects in mice. Protein Cell 4, 231–242.

Perez-Figares, J.M., Jimenez, A.J., Perez-Martin, M., Fernandez-Llebrez, P., Cifuentes, M., Riera, P., Rodriguez, S., Rodriguez, E.M., 1998. Spontaneous congenital hydrocephalus in the mutant mouse hyh. Changes in the ventricular system and the subcommissural organ. J. Neuropathol. Exp. Neurol. 57, 188–202.

Perez-Figares, J.M., Jimenez, A.J., Rodriguez, E.M., 2001. Subcommissural organ, cerebrospinal fluid circulation, and hydrocephalus. Microsc. Res. Tech. 52, 591–607.

Piper, M., Plachez, C., Zalucki, O., Fothergill, T., Goudreau, G., Erzurumlu, R., Gu, C., Richards, L.J., 2009. Neuropilin 1-Sema signalling regulates crossing of cingulate pioneering axons during development of the corpus callosum. Cereb. Cortex 19 (Suppl. 1), i11–i21.

Piper, M., Barry, G., Hawkins, J., Mason, S., Lindwall, C., Little, E., Sarkar, A., Smith, A.G., Moldrich, R.X., Boyle, G.M., Tole, S., Gronostajski, R.M., Bailey, T.L., Richards, L.J., 2010. NFIA controls telencephalic progenitor cell differentiation through

repression of the Notch effector Hes1. J. Neurosci. 30, 9127–9139.

Piper, M., Harris, L., Barry, G., Heng, Y.H., Plachez, C., Gronostajski, R.M., Richards, L.J., 2011. Nuclear factor one X regulates the development of multiple cellular populations in the postnatal cerebellum. J. Comp. Neurol. 519, 3532–3548.

Piper, M., Barry, G., Harvey, T.J., McLeay, R., Smith, A.G., Harris, L., Mason, S., Stringer, B.W., Day, B.W., Wray, N.R., Gronostajski, R.M., Bailey, T.L., Boyd, A.W., Richards, L.J., 2014. NFIB-mediated repression of the epigenetic factor Ezh2 regulates cortical development. J. Neurosci. 34, 2921–2930.

Pjanic, M., Pjanic, P., Schmid, C., Ambrosini, G., Gaussin, A., Plasari, G., Mazza, C., Bucher, P., Mermod, N., 2011. Nuclear factor I revealed as family of promoter binding transcription activators. BMC Genomics 12, 181.

Plachez, C., Lindwall, C., Sunn, N., Piper, M., Moldrich, R.X., Campbell, C.E., Osinski, J.M., Gronostajski, R.M., Richards, L.J., 2008. Nuclear factor I gene expression in the developing forebrain. J. Comp. Neurol. 508, 385–401.

Roales-Bujan, R., Paez, P., Guerra, M., Rodriguez, S., Vio, K., Ho-Plagaro, A., Garcia-Bonilla, M., Rodriguez-Perez, L.M., Dominguez-Pinos, M.D., Rodriguez, E.M., Perez-Figares, J.M., Jimenez, A.J., 2012. Astrocytes acquire morphological and functional characteristics of ependymal cells following disruption of ependyma in hydrocephalus. Acta Neuropathol. 124, 531–546.

Rodriguez, E.M., Rodriguez, S., Hein, S., 1998. The subcommissural organ. Microsc. Res. Tech. 41, 98–123.

Rogers, N., Cheah, P.S., Szarek, E., Banerjee, K., Schwartz, J., Thomas, P., 2013. Expression of the murine transcription factor SOX3 during embryonic and adult neurogenesis. Gene Expr. Patterns 13, 240–248.

Sival, D.A., Guerra, M., den Dunnen, W.F., Batiz, L.F., Alvial, G., Castaneyra-Perdomo, A., Rodriguez, E.M., 2011. Neuroependymal denudation is in progress in full-term human foetal spina bifida aperta. Brain Pathol. 21, 163–179.

Spassky, N., Merkle, F.T., Flames, N., Tramontin, A.D., Garcia-Verdugo, J.M., Alvarez-Buylla, A., 2005. Adult ependymal cells are postmitotic and are derived from radial glial cells during embryogenesis. J. Neurosci. 25, 10–18.

Steele-Perkins, G., Plachez, C., Butz, K.G., Yang, G., Bachurski, C.J., Kinsman, S.L., Litwack, E.D., Richards, L.J., Gronostajski, R.M., 2005. The transcription factor gene Nfib is essential for both lung maturation and brain development. Mol. Cell Biol. 25, 685–698.

Tissir, F., Qu, Y., Montcouquiol, M., Zhou, L., Komatsu, K., Shi, D., Fujimori, T., Labeau, J., Tyteca, D., Courtoy, P., Poumay, Y., Uemura, T., Goffinet, A.M., 2010. Lack of cadherins Celsr2 and Celsr3 impairs ependymal ciliogenesis, leading to fatal hydrocephalus. Nat. Neurosci. 13, 700–707.

Vio, K., Rodriguez, S., Yulis, C.R., Oliver, C., Rodriguez, E.M., 2008. The subcommissural organ of the rat secretes Reissner's fiber glycoproteins and CSF-soluble proteins reaching the internal and external CSF compartments. Cerebrospin. Fluid Res. 5, 3.

Wagner, C., Batiz, L.F., Rodriguez, S., Jimenez, A.J., Paez, P., Tome, M., Perez-Figares, J.M., Rodriguez, E.M., 2003. Cellular mechanisms involved in the stenosis and obliteration of the cerebral aqueduct of hyh mutant mice developing congenital hydrocephalus. J. Neuropathol. Exp. Neurol. 62, 1019–1040.

Wilson, G.R., Wang, H.X., Egan, G.F., Robinson, P.J., Delatycki, M.B., O'Bryan, M.K., Lockhart, P.J., 2010. Deletion of the Parkin co-regulated gene causes defects in ependymal ciliary motility and hydrocephalus in the quakingviable mutant mouse. Hum. Mol. Genet. 19, 1593–1602.